New WS9326A Congeners from *Streptomyces* sp. 9078 Inhibiting *Brugia malayi* asparaginyl-tRNA Synthetase

Zhiguo Yu,[†] Sanja Vodanovic-Jankovic,[⊥] Michael Kron,*[⊥] and Ben Shen*[,†,‡,§]

[†]Department of Chemistry, [‡]Department of Molecular Therapeutics, and [§]Natural Products Library Initiative at the Scripps Research Institute, the Scripps Research Institute, Jupiter, FL 33458, United State, and [⊥]Department of Pathology, Biotechnology and Bioengineering Center, and Department of Medicine, Medical College of Wisconsin, Milwaukee, WI, 53226, United States.

mkron@mcw.edu; shenb@scripps.edu

Supporting Information

General		S2
Fermentation and isolation		S2
Preparation of triacetyl-WS9326A (**1a**) and triaceyl-WS9326C (**2a**)		S2
Physico-chemical properties of **1**, **1a**, **2**, **2a**, **3**, and **4**		S2
*Bm*AsnRS inhibition assay		S3
Adult *B. malayi* worm killing assays		S4
General cytotoxicity assay with human liver cell line HepG2		S4
References		S5
Table S1	^{1}H and ^{13}C NMR data of triacetyl-WS9326A (**1a**) and triacetyl-WS9326C (**2a**) in $CDCl_3$	S6
Table S2	^{1}H and ^{13}C NMR data of WS9326A (**1**) and WS9326C (**2**) in d_6-DMSO	S8
Figure S1	*Bm*AsnRS inhibition using the pretransfer editing assay	S10
Figure S2	Adult *B. malayi* worm killing rates in vitro as measured by worm mobility	S11
Figure S3	Adult *B. malayi* worm killing rates in vitro as measured by MTT assay	S12
Figure S4	General cytotoxicity to human heptic cells as measured by MTT assay	S13
Figure S5	^{1}H NMR spectrum of WS9326A (**1**) in d_6-DMSO	S14
Figure S6	^{13}C NMR spectrum of WS9326A (**1**) in d_6-DMSO	S15
Figure S7	^{1}H NMR spectrum of triacetyl-WS9326A (**1a**) in d_6-DMSO	S16
Figure S8	^{13}C NMR spectrum of triacetyl-WS9326A (**1a**) in d_6-DMSO	S17
Figure S9	^{1}H NMR spectrum of WS9326C (**2**) in d_6-DMSO	S18
Figure S10	^{13}C NMR spectrum of WS9326C (**2**) in d_6-DMSO	S19
Figure S11	^{1}H NMR spectrum of triacetyl-WS9326C (**2a**) in $CDCl_3$	S20
Figure S12	^{13}C NMR spectrum of triacetyl-WS9326C (**2a**) in $CDCl_3$	S21
Figure S13	HSQC spectrum of triacetyl-WS9326C (**2a**) in $CDCl_3$	S22
Figure S14	HMBC spectrum of triacetyl-WS9326C (**2a**) in $CDCl_3$	S23
Figure S15	^{1}H-^{1}H COSY spectrum of triacetyl-WS9326C (**2a**) in $CDCl_3$	S24
Figure S16	NOESY spectrum of triacetyl-WS9326C (**2a**) in $CDCl_3$	S25
Figure S17	^{1}H NMR spectrum of WS9326D (**3**) in d_6-DMSO	S26
Figure S18	^{13}C NMR spectrum of WS9326D (**3**) in d_6-DMSO	S27
Figure S19	HSQC spectrum of WS9326D (**3**) in d_6-DMSO	S28
Figure S20	HMBC spectrum of WS9326D (**3**) in d_6-DMSO	S29
Figure S21	^{1}H-^{1}H COSY spectrum of WS9326D (**3**) in d_6-DMSO	S30
Figure S22	NOESY spectrum of WS9326D (**3**) in d_6-DMSO	S31
Figure S23	^{1}H NMR spectrum of WS9326E (**4**) in d_6-DMSO	S32
Figure S24	^{13}C NMR spectrum of WS9326E (**4**) in d_6-DMSO	S33
Figure S25	HSQC spectrum of WS9326E (**4**) in d_6-DMSO	S34
Figure S26	HMBC spectrum of WS9326E (**4**) in d_6-DMSO	S35
Figure S27	^{1}H-^{1}H COSY spectrum of WS9326E (**4**) in d_6-DMSO	S36
Figure S28	NOESY spectrum of WS9326E (**4**) in d_6-DMSO	S37

General

Optical rotations were measured in methanol with a Perkin-Elmer 241 instrument at the sodium D line (589 nm). ^{1}H and ^{13}C NMR spectra were recorded at 25°C with a Bruker Avance III 700 MHz ULTRAShield. High-resolution mass spectra were acquired with a Bruker Daltonics Ultra High Resolution TOF – Maxis spectrometer. Semi-preparative HPLC was performed on a Varian HPLC system with an Altima C-18 column (5 µ, 10.0 x 250 mm, Alltech, Deerfield, IL). Column chromatography was performed using either silica gel (230-400 mesh, Natland International Corporation, Research Triangle Park, NC) or Sephadex LH-20 (Pharmacia, Kalamazoo, MI). All chemical reagents were purchased from Sigma-Aldrich and used without further purification.

Fermentation and isolation

The *Streptomyces* sp. 9078 was preserved as a spore solution at -80^{o}C. A two-stage fermentation was performed, and for both stages F medium (i.e., sucrose, 100 g, glucose, 10 g, casamino acids, 0.1 g; yeast extract, 5 g; MOPS, 21 g, trace elements, 1 mL, K_2SO_4, 0.25 g, $MgCl_2$-$6H_2O$, 10 g, in a final volume of 1.0-L H_2O, pH 7.0) was used. Thus, a 250-mL baffled Erlenmeyer flask, containing 50 mL of the F medium, was inoculated with 10 µL of the *S*. sp.9078 spore solution and incubated with shaking (250 rpm) at 28.0°C for 2 days to prepare the seed culture. Twenty-four 2-L baffled Erlenmeyer flasks, each contains 400 mL of F medium, were then inoculated with 20 mL of the seed culture and left for fermentation for 7 days under identical conditions.

The production cultures were centrifuged at 5,000 rpm and 4°C for 30 min to remove mycelia, and the broth was extracted with 3% Amberlite XAD16 resin for 4 hours at room temperature with agitation. Resin was harvested by centrifugation and eluted three times with methanol. The combined methanol elution was then concentrated under reduced pressure to afford the crude extract.

The crude extract (3.2 g) was subjected to silica gel chromatography eluted step wisely with $CHCl_3$:CH_3OH (100:0, 50:1, 20:1, 10:1, 5:1 and 0:100, 1-L each) as the mobile phase to afford six fractions, F1 to F6. Fraction F5 (187 mg) was further chromatographed over Sephadex LH-20 column and eluted with CH_3OH to yield three sub-fractions F5A, F5B and F5C. Subfraction F5B was finally purified by semipreparative HPLC to afford **1** (13.1 mg), **2** (5.2 mg), **3** (3.9 mg), and **4** (3.2 mg) as white powders.

Preparation of triacetyl-WS9326A (1a) and triacetyl-WS9326C (2a)

The preparation of triacetyl-WS9326A (1a) and triacetyl-WS9326C (2a) followed literature procedures.[1] Thus to a solution of WS9326A or WS9326C (3 mg) in pyridine (0.5 mL) were added acetic anhydride (0.1 mL), and the reaction mixture was allowed to stand at room temperature overnight. The reaction mixture was evaporated to dryness, affording an oily residue that was purified by preparative TLC [$CHCl_3$-MeOH (10:1)]. The final TLC-purified product was triturated with diethyl ether to give triacetyl-WS9326A (3.1 mg) and triacetyl-WS9326C (2.9 mg) as a white powder, respectively.

Physico-chemical properties of 1, 1a, 2, 2a, 3, and 4

WS9326A (**1**): white powder; $[\alpha]^{20}_{D}$ -89.0° (c 1.00, MeOH); HRESIMS for the $[M + H]^+$ ion at *m/z* 1037.4984 (calculated $[M + H]^+$ ion for $C_{54}H_{68}N_8O_{13}$ at *m/z* 1037.4983); ^{1}H and ^{13}C NMR data, see Tables S2. The optical rotation of **1** agreed well with that of $[\alpha]^{23}_{D}$ -84.0° (c 1.00, MeOH)[2] reported previously, confirming that they share the same absolute stereochemistry.

Triacetyl-WS9326A (**1a**): white powder; HRESIMS for the $[M + H]^+$ ion at *m/z* 1063.5321 (calculated $[M + H]^+$ ion for $C_{60}H_{74}N_8O_{16}$ at *m/z* 1063.5300); ^{1}H and ^{13}C NMR data, see Table S1.

WS9326C (**2**): white powder; $[\alpha]^{20}_{D}$ -114.0° (c 1.00, MeOH); HRESIMS for the $[M + H]^+$ ion at *m/z* 1023.4842 (calculated $[M + H]^+$ ion for $C_{53}H_{66}N_8O_{13}$ at *m/z* 1023.4827); ^1H and ^{13}C NMR data, see Tables S2.

Triacetyl-WS9326C (**2a**): white powder; HRESIMS for the $[M + H]^+$ ion at *m/z* 1049.5152 (calculated $[M + H]^+$ ion for $C_{59}H_{72}N_8O_{16}$ at *m/z* 1049.5144); ^1H and ^{13}C NMR data, see Table S1, as well as Table 1.

WS9326D (**3**): white powder; $[\alpha]^{20}_{D}$ -26.7° (c 0.69, MeOH); HRESIMS for the $[M + H]^+$ ion at *m/z* 854.4357 (calculated $[M + H]^+$ ion for $C_{47}H_{59}N_5O_{10}$ at *m/z* 854.4340); ^1H and ^{13}C NMR data, see Table 1.

WS9326E (**4**): white powder; $[\alpha]^{20}_{D}$ -44.0° (c 0.85, MeOH); HRESIMS for the $[M + H]^+$ ion at *m/z* 840.4194 (calculated $[M + H]^+$ ion for $C_{46}H_{57}N_5O_{10}$ at *m/z* 840.4183); ^1H and ^{13}C NMR data, see Table 1.

*Bm*AsnRS inhibition assay

*Bm*AsnRS inhibition assays were carried out according to our recently published procedure.[3] This nonradioactive assay measures phosphate generated by the recombinant *Bm*AsnRS and capitalizes on the fact that the first step of the two step aminoacylation reaction does not require tRNA to generate the pyrophosphate substrate of bacterial pyrophosphatase. Inorganic phosphate produced by the pyrophosphatase is readily detected by reaction with malachite green and absorption monitoring at 620 nm. The assay exploits the asparagine substrate mimetic L-aspartate β-hydroxamate and has been optimized for HTS of microbial extracts using both recombinant *B. malayi* and human AsnRS.

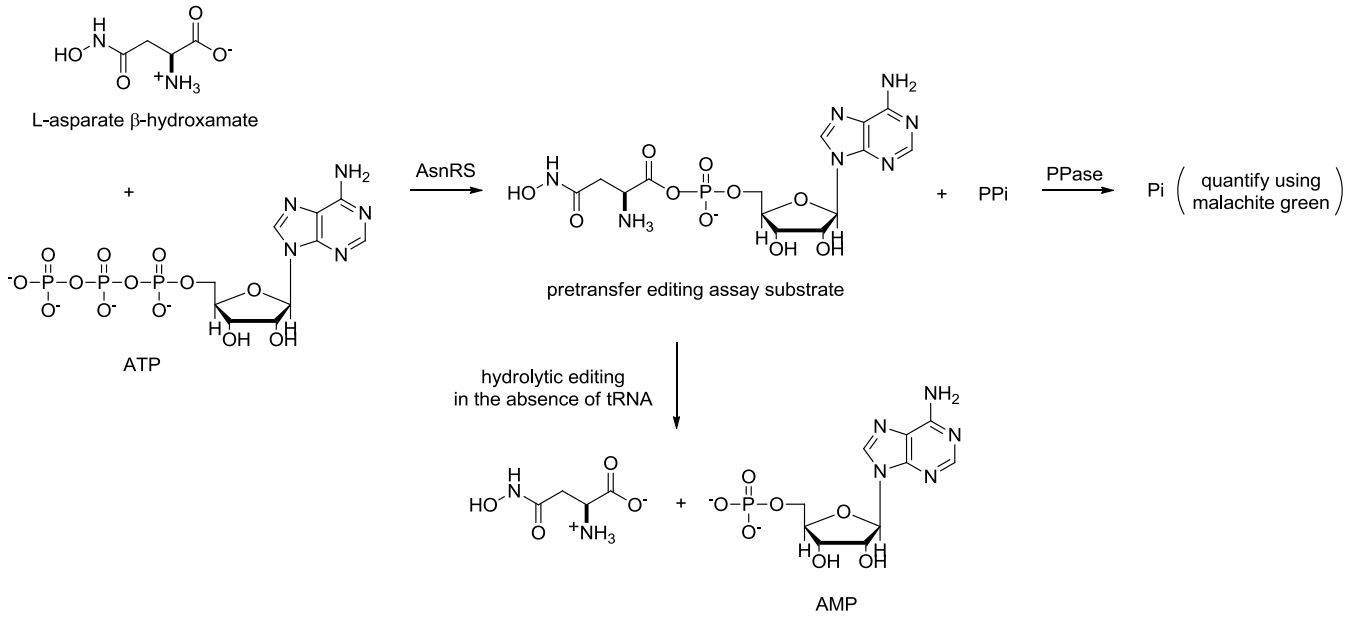

Thus, in the 96 well-plate format, the assay conditions were as follows: 50 mM Hepes, pH 7.4, 25 mM $Mg(C_2H_3O_2)_2$, 0.2 mM ATP, 1 U/ml PPase, 20 mM L-Cys, 5 mM DTT, 0.38 mM AsnRS, and WS9326A (**1**), WS9326C (**2**), WS9326D (**3**), or WS9326E (**4**), as well as TAM B[4] as a positive control. Enzyme and inhibitors were incubated for 10 minutes before addition of L-aspartate β-hydroxamate (0.2 mM final concentration). The reaction was then incubated 37°C for 3 hours before adding 50 μL of the malachite green reagent containing 0.0876% malachite green hydrochloride, 0.05% Triton X-100, and 2.8% ammonium molybdate tetrahydrate in 0.7 N H_2SO_4. The resultant mixture was then incubated at room temperature for 10 minutes, and the absorption at 620 nm was finally measured using the LJL Analyst AD 96-384 plate reader (Molecular Devices, Sunnyvale, CA). Figure S1 depicted relative inhibition of BmAsnRS by each of the compounds measured at 100 μM concentration. By varying the

concentrations of **3**, **4**, and TAM B, the IC_{50}s were estimated to be 50 μM for **3**, 75 mM for 4, and 30 μM for TAM B.[4]

Adult *B. malayi* killing assays

In vitro killing (motility). Adult *B. malayi* worm killing assays were carried out according to previously published procedures.[4] In brief, live adult *B. malayi*, obtained from the NIH NIAID Filariasis Research Repository Resource facilities (FR3, Athens, GA), were transferred to 6-well-plates (3 worms, male or female per well) containing fresh RPMI 1640 culture medium supplemented with L-glutamine and penicillin/streptomycin. AsnRS inhibitors, dissolved in 100% DMSO, were diluted serially with RPMI media to obtain a varying concentration, ranging from 10 nM to 100 μM, in 0.1% DMSO. The parasites were incubated in the presence of the AsnRS inhibitors at 37^0C in 5% CO_2 atmosphere for up to ten days. When worms became immobilized (presumed dead) they were then transferred to fresh medium for ~2 hr to examine any reversal in motility of a worm under a stereozoom dissecting microscope (NIKON, JAPAN). Control groups are subjected to 1% DMSO alone as negative controls (alive for up to three weeks *in vitro*) or 100 μM albendazole, a well-known antifilarial compound that kills worm within 14 days, as positive controls. The movement and mortality of the worm can be monitored every 24 h for up to 20 days; worms in control wells are generally fully motile and assume a coiled morphology whereas dead worms are clearly immobile and assume an elongated morphology. Figure S2 depicted adult *B. malayi* warm killing rates in vitro with varying concentration of **3** (ranging from 10 nM to 50 μM) in comparison with 100 μM albendazole and 50 μM TAM B as positive controls as measured by warm mobility and morphology.

In vitro killing (mitochondrial enzyme inactivity/cell death). The 3-(4,5-dimethylthiazol-2-yl)-2,5-diphenyl-2H-tetrazolium bromide (MTT) assay assesses quantitatively the viability of worms that appear to be dead or dying as opposed to those just paralyzed (immobile).[4,5] Briefly, after observing motility of the parasite, MTT assays were performed with the same parasite (drug treated vs. untreated) as reported in Figure S2. The worms were washed in PBS pH 7.2, quickly blotted over a filter disc, and immediately transferred to 96-well-plate containing 0.1 mL MTT (0.5 mg/mL in PBS, pH 7.2). The plate was incubated at 37^0C for 45 minutes and each worm was transferred to 0.1 mL of DMSO in another 96-well-plate that was left at 37^0C for 45 minutes for solubilization of blue formazan (reduced product of MTT). The worms were removed and the plate was gently agitated to disperse the color evenly and the absorbance of the solubilized formazan was measured at 510 nm using a multi-well-plate-reader (Tecan) against the DMSO blank. The absorbance value of each well was compared with the mean value of control wells. Percent inhibition in MTT reduction by the treated parasite over that of untreated control worm was calculated. Figure S3 depicted adult *B. malayi* warm killing in vitro with varying concentration of **3** (ranging from 5, 10, and 50 μM) in comparison with 100 μM albendazole and 50 μM TAM B as positive controls as measured by the MTT assay.

General cytotoxicity assay with human liver cell line HepG2

MTT conversion to formazan can be also used for general cytotoxicity testing with the human liver cell line, HepG2. Tissue cultures of human Hep G2 liver cells were incubated with 100 μM **3** or 100 μM TAM B, with 100 μM AT1, a known actinomycete toxin, as a positive control, for 24 hours before measurement of mitochondrial enzyme activity. Cell viability/metabolic activity is assessed after addition of MTT and measured by spectrophotometry. Values reported are from background absorbance at OD 690 nm subtracted from absorbance at OD 570 nm. Figure S4 depicted the general cytotoxicity to human hepatic cells by **3** and TAM B with the control. Cytoxicity is defined at >50% cell death, and **3** demonstrated ~25% cell death at 100 μM.

References

(1) Shigematsu, N.; Hayashi, K.; Kayakiri, N.; Takase, S.; Hashimoto, M.; Tanaka, H. *J. Org. Chem.* **1993**, *58*, 170-175.

(2) Hayashi, K.; Hashimoto, M.; Shigematsu, N.; Nishicawa, M.; Ezaki, M.; Yamashita, M.; Kiyoto, S.; Okuhara, M.; Kohsaks, M.; Imanaka, H. *J. Antibiot.* **1992**, *45*, 1055-1063

(3) Danel, F.; Caspers, P.; Nuoffer, C.; Hartlein, M.; Kron, M. A.; Page, M. G. *Curr. Drug Discovery Technol.* **2010**, *8*, 66-75.

(4) Yu, Z.; Vodanovic-Jankovic, S.; Ledeboer, N.; Huang, S.; Rajski, S. R.; Kron, M.; Shen, B. *Org. Lett.* **2011**, *13*, 2034-2037.

(5) Comley, J. C. W.; Res, M. J.; Turner, C. H.; Jenkins, D. C. *Int. J. Parastol.*, **1989**, *19*, 77-83.

Table S1. ^{1}H (700 MHz) and ^{13}C (175 MHz) NMR data of triacetyl-WS9326A (**1a**) and triacetyl-WS9326C (**2a**) in $CDCl_3$[a]

position[b]		**2a**		**1a**	
		δ_H (J in Hz)	δ_C	δ_H (J in Hz)	δ_C
Acyl	1		166.1 s		166.4 s
	2	6.98, 1H, d (16.0)	121.2 d	6.78, 1H, d (15.6)	121.0 d
	3	7.91, 1H, d (16.0)	140.0 d	7.91, 1H, d (15.6)	140.5 d
	1’		133.6 s		133.5 s
	2’	7.56, 1H, d (7.80)	126.3 d	7.53, 1H, d (7.70)	126.2 d
	3’	7.18, 1H, t (7.60)	127.0 d	7.18, 1H, t (7.28)	127.0 d
	4’	7.29, 1H[c]	128.9 d	7.32, 1H[e]	129.0 d
	5’	7.20, 1H, d (7.80)	130.0 d	7.20, 1H, d (7.60)	129.9 d
	6’		138.4 s		138.5 s
	1’’	6.55, 1H, d (11.4)	126.9 d	6.51, 1H, d (11.5)	126.8 d
	2’’	5.80, 1H, dt (11.5, 7.40)	134.9 d	5.78, 1H, dt (11.5, 7.40)	135.0 d
	3’’	2.00, 2H, m	30.5 t	1.96, 2H, m	30.5 t
	4’’	1.35, 2H, m	22.7 t	1.32, 2H, m	22.6 t
	5’’	0.80, 3H, t (7.50)	13.8 q	0.76, 3H, t (7.00)	13.7 q
[1]Ser/[1]Thr	NH	7.65, 1H, d (7.80)		7.61, 1H, d (8.40)	
	α	5.45, 1H, m	50.9 d	5.50, 1H, d, (8.50)	52.8 d
	β	4.43, 1H, m	63.8 t	5.47, 1H, m	71.0 d
		4.68, 1H, m			
	γ			1.40, 3H, d (6.30)	17.1 q
	CO		169.5 s		169.4 s
[2]ΔMeTyr	NMe	3.57, 3H, s	40.4 q	3.59, 3H, s	39.7 q
	α		138.8 s		138.9 s
	β	6.84, 1H, s	128.2 d	6.73, 1H, s	126.7 d
	1		131.0 s		131.1 s
	2,6	7.29, 2H[c]	129.9 d	7.32, 2H[e]	129.9 d
	3,5	7.05, 2H[d]	121.9 d	7.04, 2H[f]	122.0 d
	4		150.9 s		150.8 s
	CO		166.0 s		165.7 s
	CO (Ac)		169.6 s		169.7 s
	Me (Ac)	2.30, 3H, s	21.1 q	2.29, 3H, s	21.1 q
[3]Leu	NH	8.08, 1H, d (8.20)		7.45, 1H, d (8.00)	
	α	4.45, 1H, m	51.1 d	4.56, 1H, m	52.5 d
	β	1.28, 1H, m	38.0 t	1.24, 1H, m	39.2 t
		1.64, 1H, m		1.66, 1H, m	
	γ	1.00, 1H, m	24.2 d	0.94, 1H, m	24.2 d
	δ	0.71, 3H, d (6.60)	23.0 q	0.65, 3H, d (6.50)	22.9 q
		0.79, 3H, d (7.10)	21.5 q	0.77, 3H, d (6.60)	21.5 q
	CO		170.9 s		170.4 s
[4]Phe	NH	7.94, 1H, d (8.10)		8.23, 1H, d (7.50)	
	α	4.70, 1H, m	54.9 d	4.63, 1H, dd (14.4, 7.60)	55.9 d
	β	2.79, 1H, m	36.7 t	2.93, 2H, m	38.0 t
		3.13, 1H, dd (13.8, 8.20)			
	1		137.2 s		137.1 s
	2,6	7.12, 2H, d (7.50)	128.2 d	7.06, 2H, d (7.60)	129.1 d
	3,5	6.99, 2H, t (7.70)	128.4 d	6.92, 2H, t (7.30)	128.6 d
	4	7.05, 1H[d]	126.5 d	7.04, 1H[f]	126.7 d
	CO		173.4 s		173.1 s
[5]*allo*Thr	NH	7.27, 1H, d (8.40)		7.69, 1H, d (9.00)	
	α	4.93, 1H, dd (8.10, 3.60)	56.0 d	4.37, 1H, m	57.9 d

	β	5.28, 1H, m	69.1 d	4.99, 1H, m	69.0 d
	γ	1.18, 3H, d (6.60)	15.1 q	1.16, 3H, d (6.50)	16.1 q
	CO		168.1 s		168.8 s
	CO (Ac)		170.5 s		170.9 s
	Me (Ac)	1.79, 3H, s	20.7 q	1.89, 3H, s	20.9 q
[6]Asn	NH	7.65, 1H, d (7.80)		7.13, 1H, d (7.60)	
	α	4.86, 1H, td (9.00, 4.40)	49.3 d	4.90, 1H, m	49.1 d
	β	2.63, 1H, dd (15.2, 4.30)	36.0 t	2.48, 1H, dd (16.0, 5.50)	35.4 t
		2.81, 1H, m		3.03, 1H, dd (16.0, 4.10)	
	γCO		173.1 s		173.1 s
	CO		173.4 s		173.2 s
[7]Ser	NH	7.19, 1H, d (7.21)		6.87, 1H, d (5.81)	
	α	4.26, 1H, dd (11.3, 5.30)	52.7 d	4.38, 1H, m	51.7 d
	β	4.42, 1H, m	62.4 t	4.33, 1H, dd (10.3, 8.30)	63.0 t
		4.58, 1H, dd (13.2, 7.70)		4.52, 1H, m	
	CO		170.2 s		168.1 s
	CO (Ac)		170.9 s		170.9 s
	Me (Ac)	2.06, 3H, s	20.8 q	2.03, 3H, s	20.8 q

[a]Assignments were based on COSY, HSQC, HMBC, and NOESY experiments
[b]Numbering followed literature precedence[1]
[c-f]Overlapping signals

Table S2. ^{1}H (700 MHz) and ^{13}C (175 MHz) NMR data of WS9326A (**1**) and WS9326C (**2**) in d_6-DMSO[a,b]

position[c]		**2**		**1**	
		δ_H (J in Hz)	δ_C	δ_H (J in Hz)	δ_C
Acyl	1		163.9 s		165.3 s
	2	6.65, 1H, d (15.7)	123.7 d	6.68, 1H, d (15.7)	122.6 d
	3	7.39, 1H[d]	136.7 d	7.42, 1H, d (15.7)	137.5 d
	1’		133.1 s		133.0 s
	2’	7.70, 1H, d (6.58)	128.1 d	7.55, 1H, d (7.80)	129.0 d
	3’	7.23, 1H[e]	128.2 d	7.27, 1H, t (7.28)	128.0 d
	4’	7.28, 1H[e]	127.9 d	7.32, 1H[f]	129.1 d
	5’	7.24, 1H[e]	127.1 d	7.35, 1H[f]	126.9 d
	6’		137.1 s		137.0 s
	1’’	6.46, 1H, d (11.5)	126.8 d	6.50, 1H, d (11.3)	127.3 d
	2’’	5.81, 1H, dt (11.5, 7.35)	134.1 d	5.83, 1H, dt (11.5, 7.41)	134.1 d
	3’’	2.04, 2H, m	29.9 t	1.98, 2H, m	29.9 t
	4’’	1.36, 2H, m	22.1 t	1.36, 2H, m	22.0 t
	5’’	0.82, 3H, t (7.28)	13.6 q	0.80, 3H, t (7.32)	13.6 q
[1]Ser/[1]Thr	NH	8.31, 1H, brs		8.71, 1H, d (9.32)	
	α	5.30, 1H, m	50.3 d	5.33, 1H, t, (9.72)	53.3 d
	β	3.83, 1H, m	62.8 t	5.03, 1H, m	73.3 d
		4.41, 1H, brd (10.1)			
	γ			1.15, 3H, d (6.28)	16.6 q
	CO		170.2 s		169.1 s
[2]ΔMeTyr	NMe	2.80, 3H, s	32.9 q	2.98, 3H, s	34.3 q
	α		138.7 s		138.7 s
	β	6.79, 1H, s	127.9 d	6.13, 1H, s	131.5 d
	1		131.2 s		128.5 s
	2,6	6.98, 2H, brs	130.0 d	7.38, 2H[f]	131.7 d
	3,5	6.52, 2H, d (7.84)	114.4 d	6.59, 2H, d (7.80)	114.8 d
	4		157.5 s		158.2 s
	CO		168.6 s		165.7 s
[3]Leu	NH	8.60, 1H, brs		9.24, 1H, d (8.00)	
	α	3.77, 1H, m	53.7 d	4.07, 1H, m	53.8 d
	β	0.95, 2H, m	38.4 t	1.26, 2H, m	39.0 t
	γ	0.69, 1H, m	23.3 d	0.85, 1H, m	22.0 d
	δ	0.55, 3H, d (5.88)	22.3 q	0.63, 3H, d (6.64)	23.4 q
		0.47, 3H, d (6.02)	22.0 q	0.75, 3H, d (6.28)	22.0 q
	CO		171.2 s		172.2 s
[4]Phe	NH	8.83, 1H, d (8.26)		7.62, 1H, d (9.40)	
	α	4.24, 1H, m	55.2 d	4.34, 1H, m	55.8 d
	β	2.69, 1H, m	35.7 t	2.73, 1H, m	36.4 t
		3.33, 1H, brd (12.6)		3.29, 1H, m	
	1		137.5 s		137.0 s
	2,6	7.22, 2H[e]	128.9 d	7.20, 2H[g]	126.1 d
	3,5	7.20, 2H, t (7.28)	128.1 d	7.27, 2H, t (7.30)	129.1 d
	4	7.39, 1H[d]	131.6 d	7.21, 1H[g]	129.6 d
	CO		172.6 s		168.9 s
[5]*allo*Thr	NH	8.24, 1H, brs		9.16, 1H, d (8.08)	
	α	4.56, 1H, m	57.5 d	4.36, 1H, m	57.2 d
	β	3.50, 1H, m	70.0 d	4.27, 1H, m	68.2 d
	γ	1.06, 3H, brs	20.4 q	0.64, 3H, d (6.16)	23.0 q
	CO		171.0 s		170.3 s

[6]Asn	NH	8.93, 1H, brs		8.33, 1H, d, (7.32)	
	α	4.86, 1H, m	51.5 d	4.45, 1H, m	50.9 d
	β	2.43, 1H, m	36.1 t	2.43, 1H, m	36.7 t
		2.69, 1H, m		2.70, 1H, m	
	γCO		171.4 s		171.3 s
	CO		172.2 s		171.7 s
[7]Ser	NH	8.39, 1H, d (7.70)		8.49, 1H, d (9.64)	
	α	4.34, 1H, m	55.6 d	4.34, 1H, m	56.0 d
	β	3.62, 1H, m	61.3 t	3.26, 1H, m	60.8 t
		3.66, 1H, m		3.17, 1H, m	
	CO		170.5 s		170.0 s

[a]Assignments were based on COSY, HSQC, HMBC, and NOESY experiments,
[b]Major conformer exists in d_6-DMSO
[c]Numbering followed literature precedence[1]
[d-g]Overlapping signals

Figure S1. *Bm*AsnRS inhibition using the pretransfer editing assay measured at 100 μM concentration of WS9326A (**1**), WS9326C (**2**), WS9326D (**3**), and WS9326E (**4**) with DMSO as a negative control and TAM B as a positive control. The IC_{50}s for the active inhibitors were estimated to be 50 μM for WS9326D (**3**), 75 μM for WS9326D (**4**), and 30 μM for TAM B.

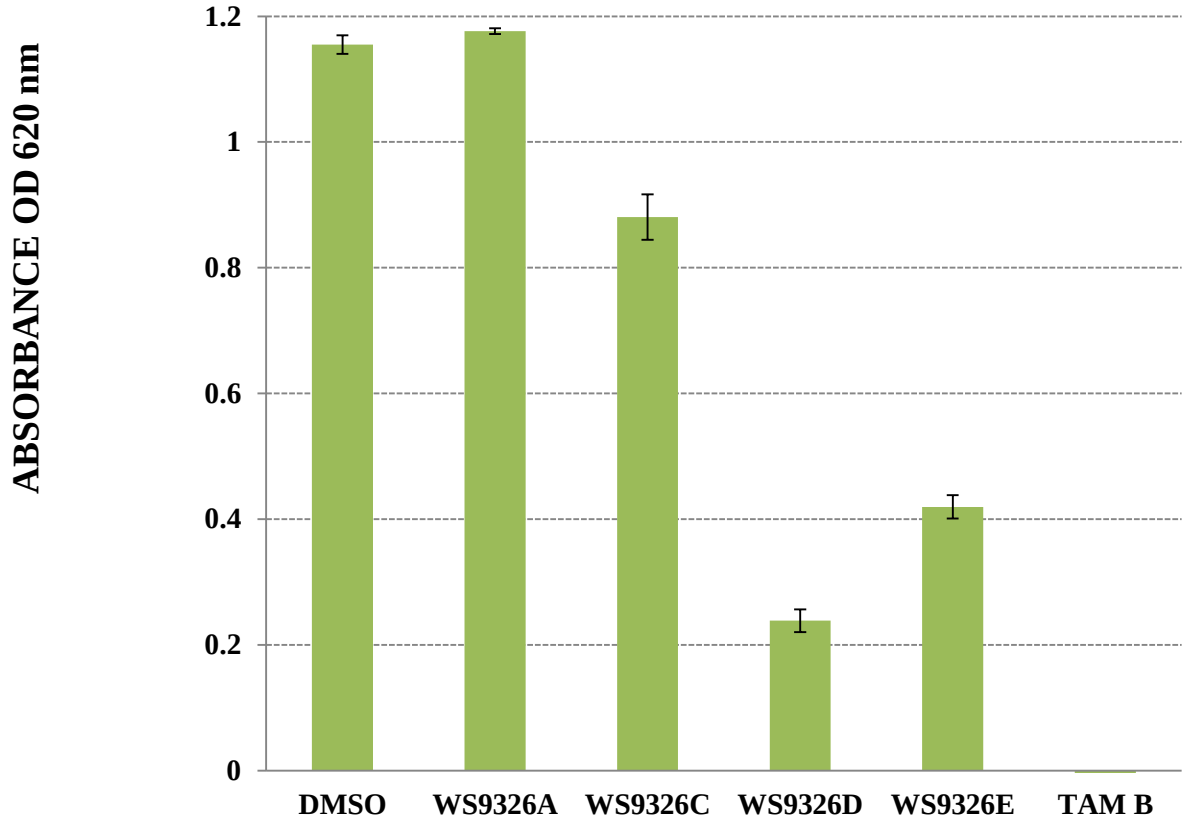

Figure S2. Adult *B. malayi* worm killing rates in vitro with varying concentration of WS9326D (**3**) (ranging from 10 nM to 50 μM) in comparison with DMSO as a negative control and 100 μM albendazole and 50 μM TAM B as positive controls as measured by warm mobility and morphology assay.

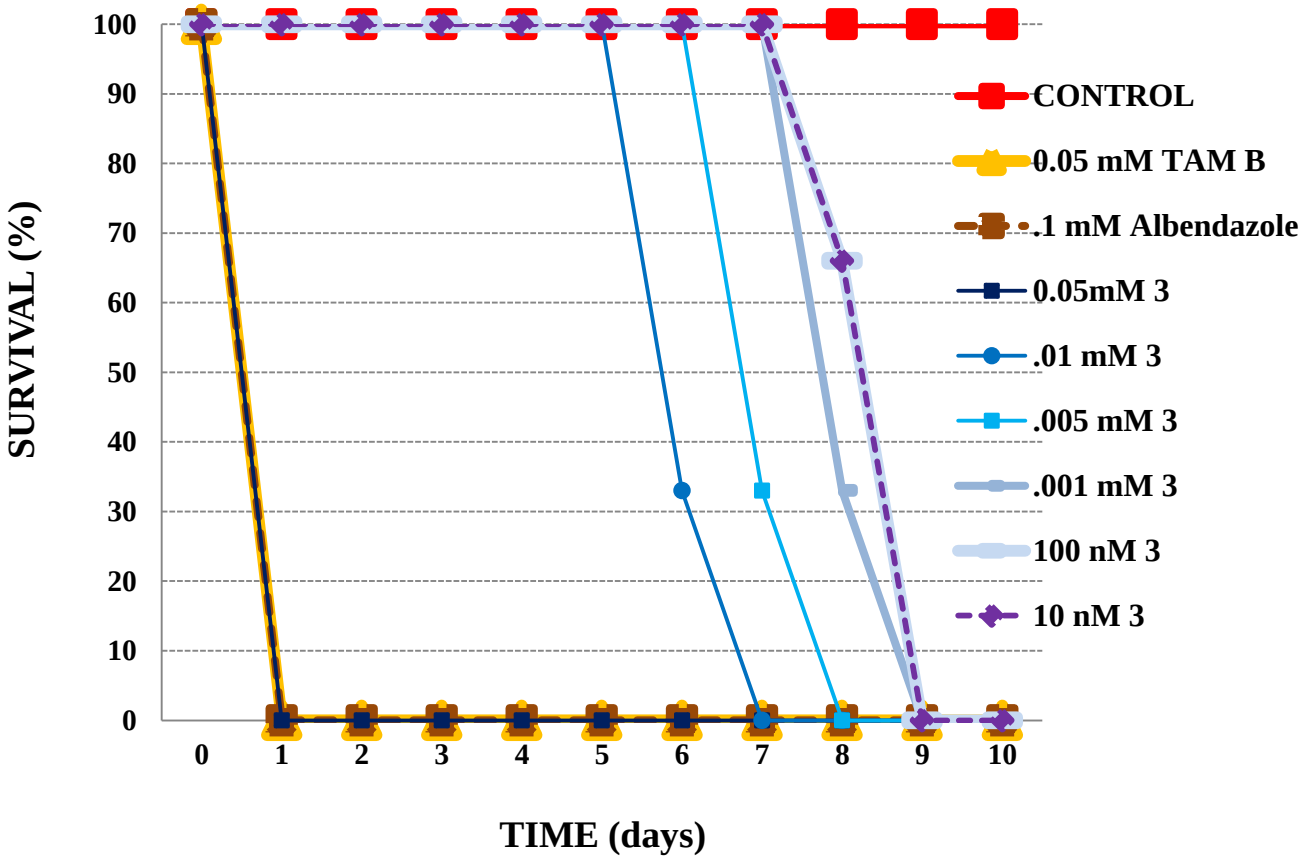

Figure S3. Adult *B. malayi* worm killing rates in vitro with varying concentration of WS9326D (**3**) (ranging from 5, 10, and 50 μM) in comparison with 100 μM albendazole and 50 μM TAM B as positive controls and DMSO as a negative control as measured by the MTT assay.

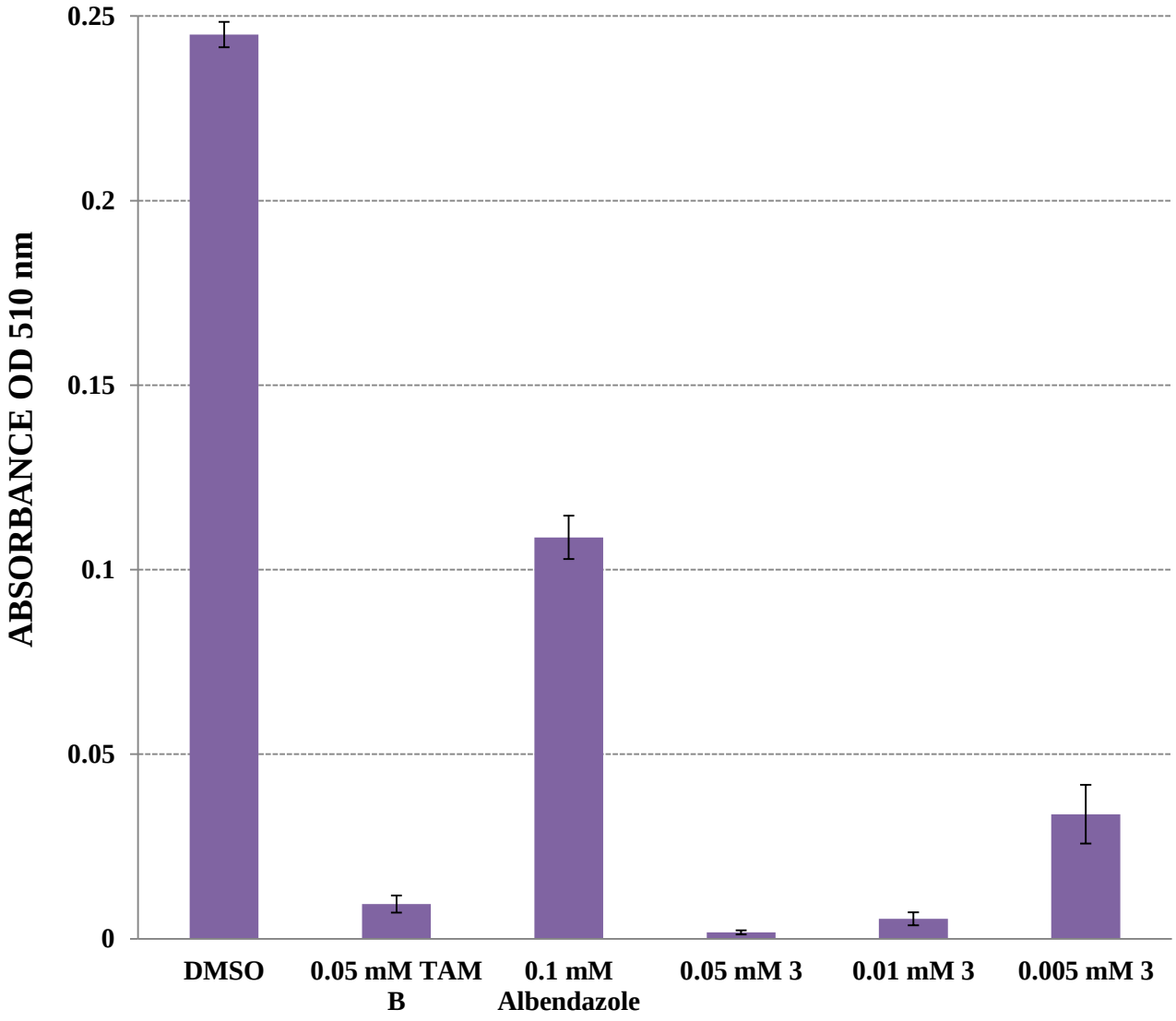

Figure S4. General cytotoxicity to human hepatic cells by WS9326D (**3**) and TAM B with DMSO as a negative control and a known actinomycete toxin (AT1) as a positive control as measured by the MTT assay. Cytoxicity is defined at >50% cell death, and **3** demonstrated ~25% cell death at 100 μM.

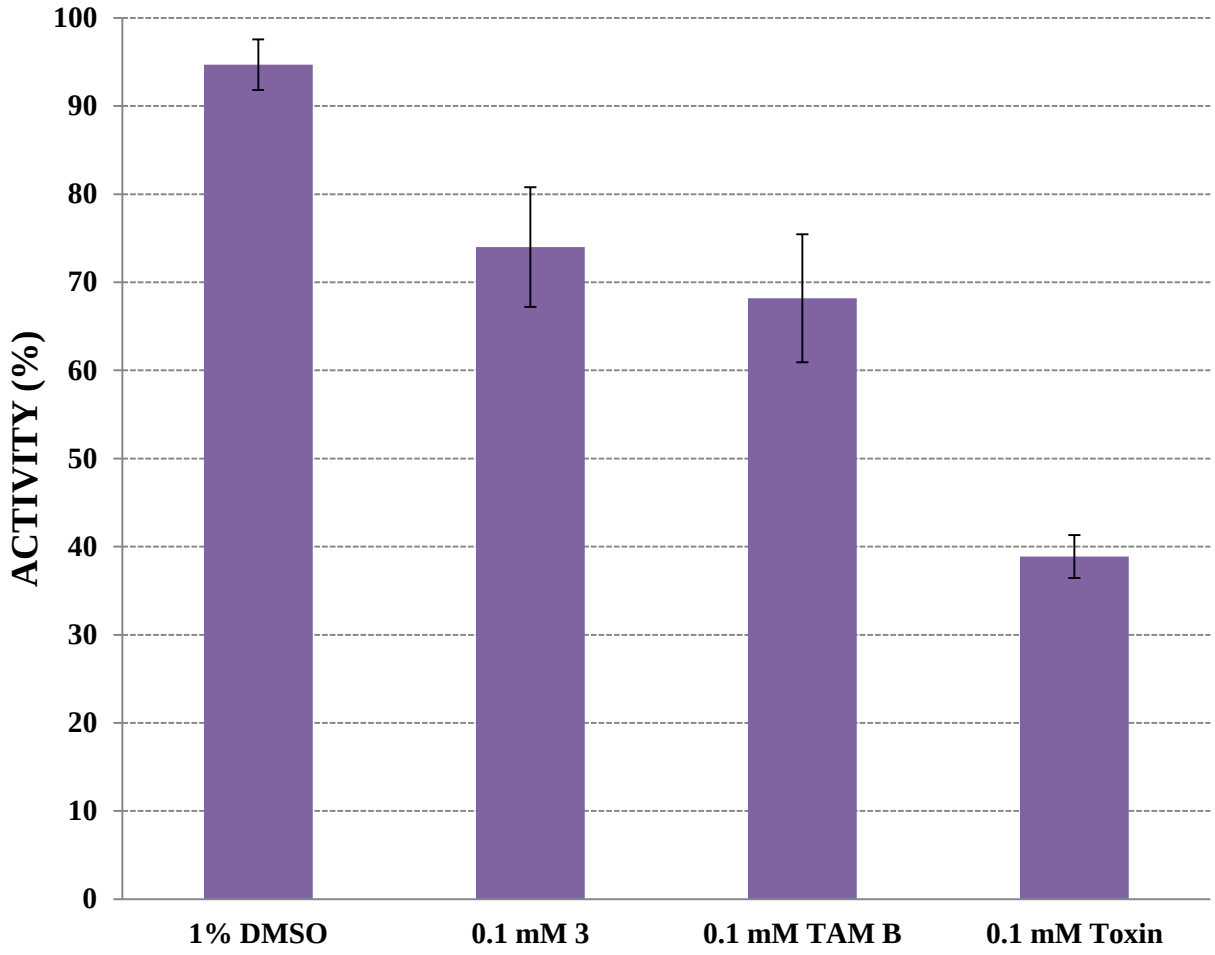

Figure S5. ^{1}H (700 MHz) NMR spectrum of WS9326A (**1**) in d_6-DMSO

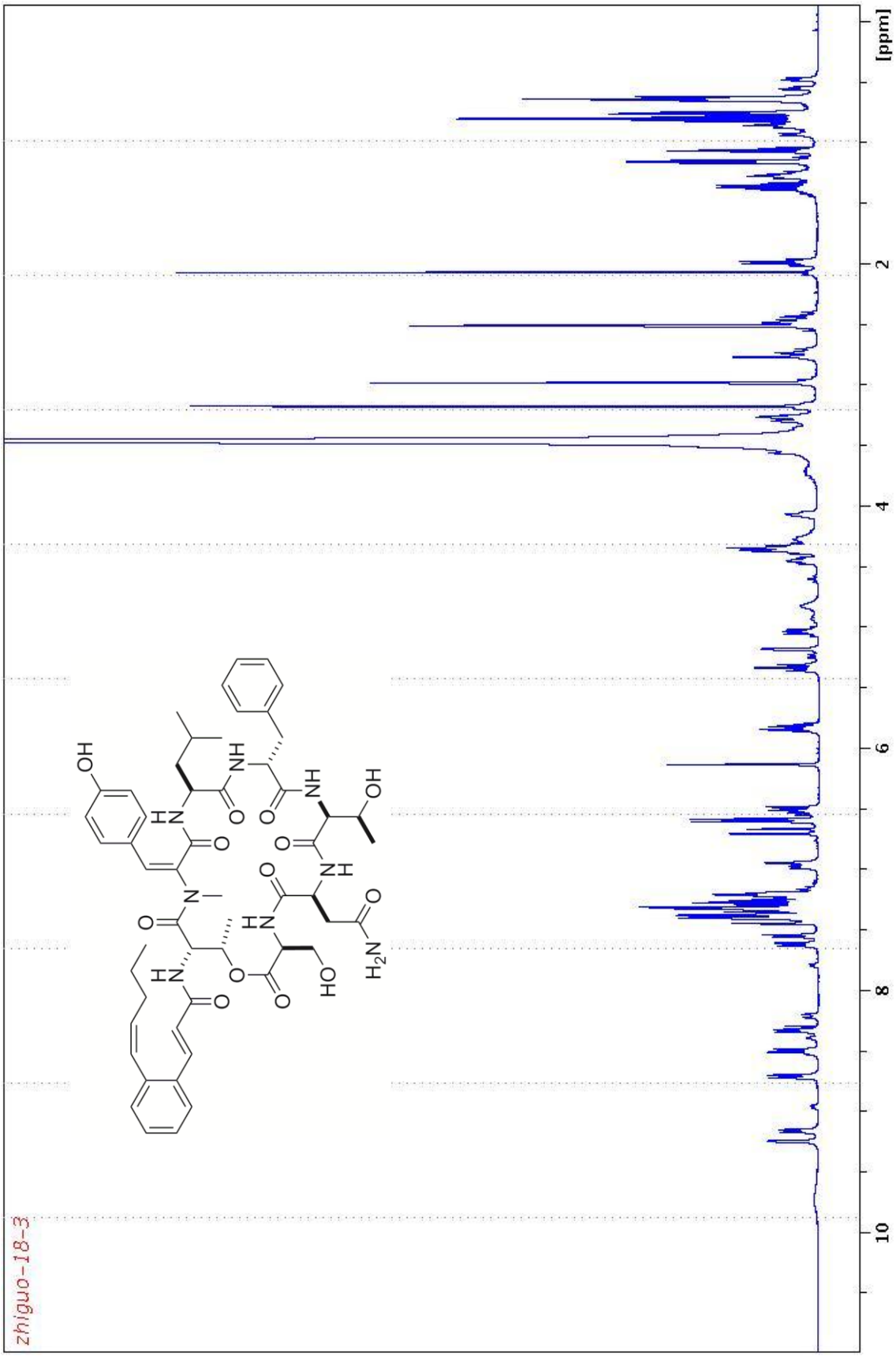

Figure S6. ^{13}C (175 MHz) NMR spectrum of WS9326A (**1**) in d_6-DMSO

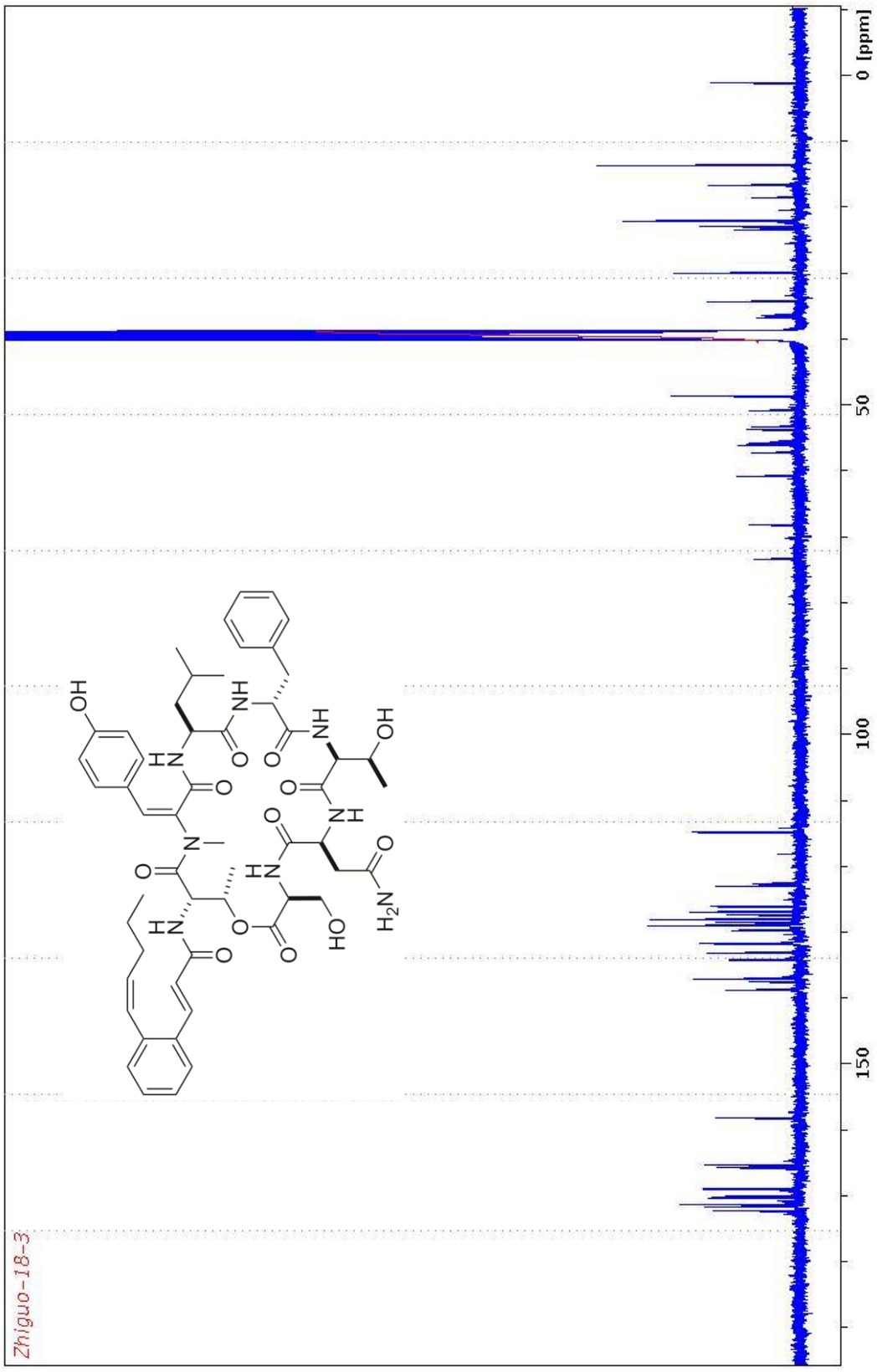

Figure S7. ^{1}H (700 MHz) NMR spectrum of triacetyl-WS9326A (**1a**) in $CHCl_3$

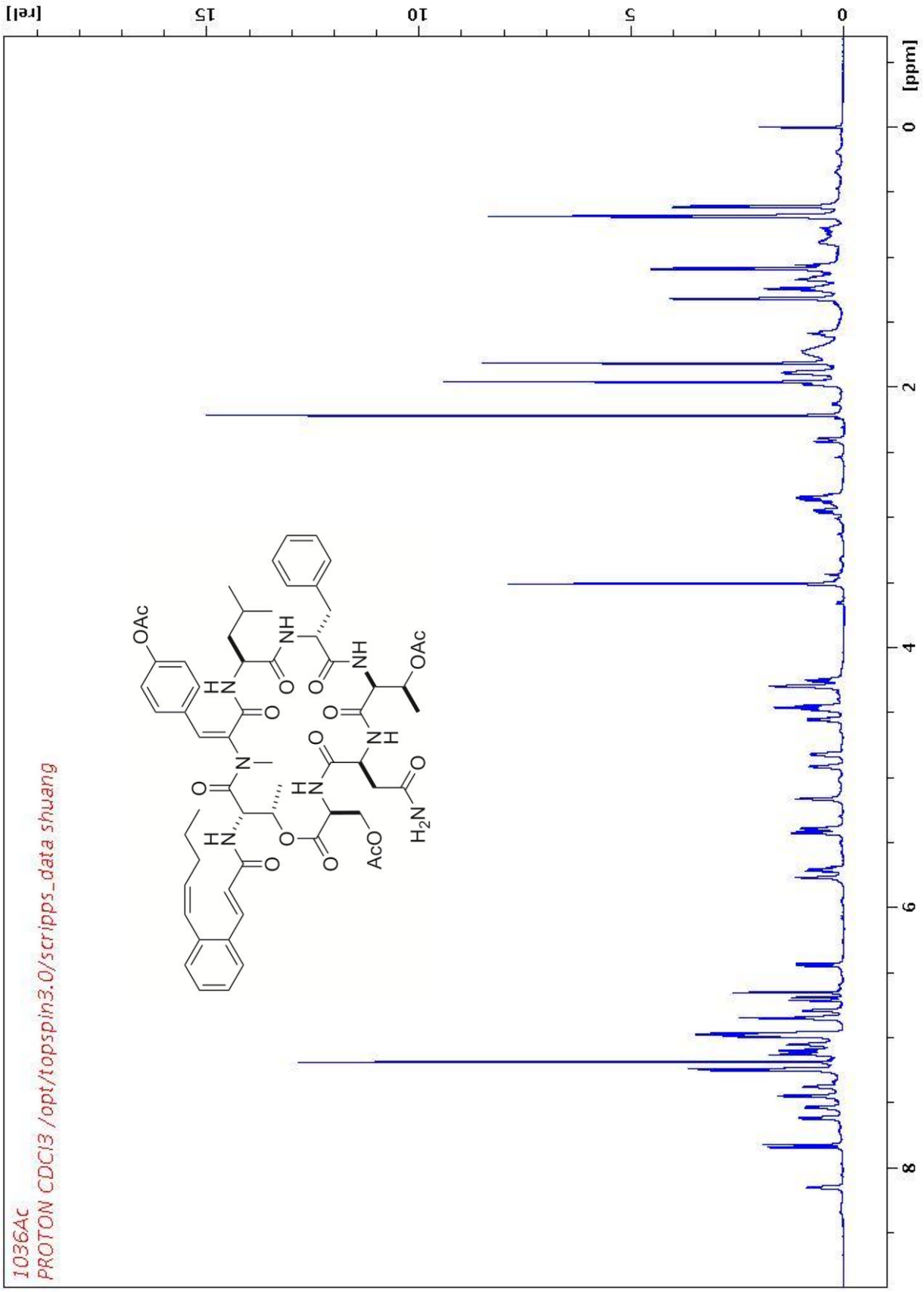

Figure S8. ^{13}C (175 MHz) NMR spectrum of triacetyl-WS9326A (**1a**) in $CDCl_3$

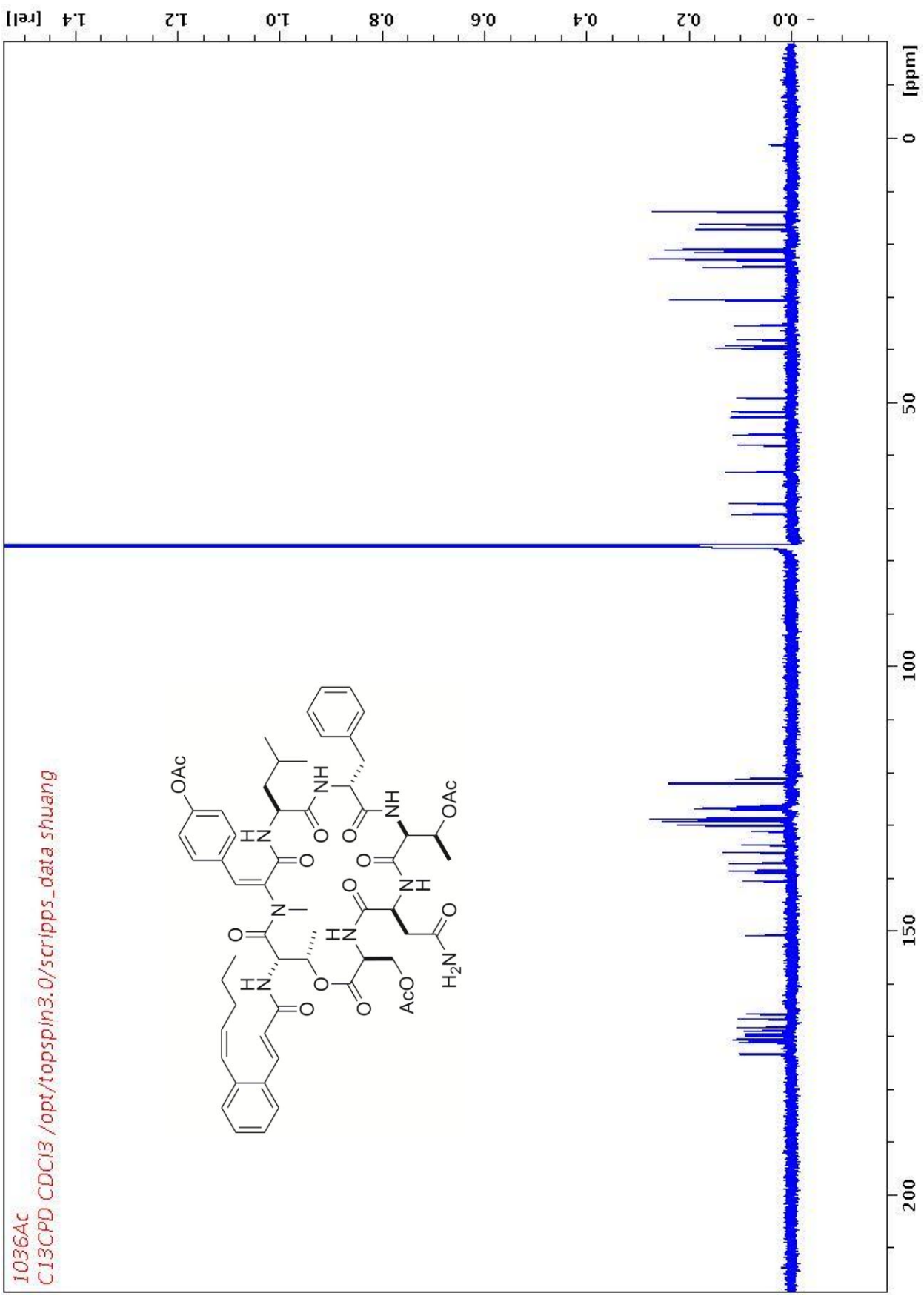

Figure S9. ^{1}H (700 MHz) NMR spectrum of WS9326C (**2**) in d_6-DMSO

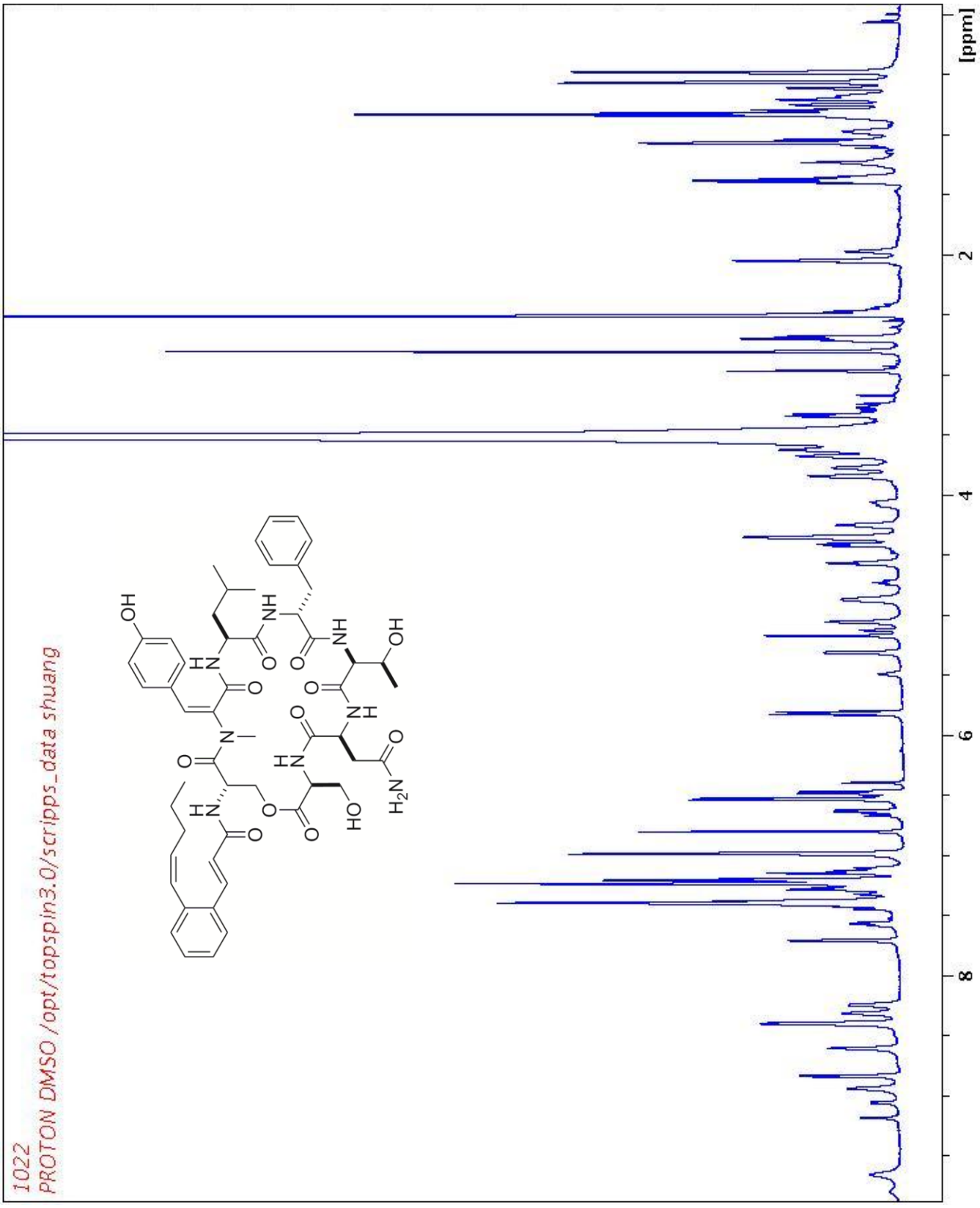

Figure S10. ^{13}C (175 MHz) NMR spectrum of WS9326C (**2**) in d_6-DMSO

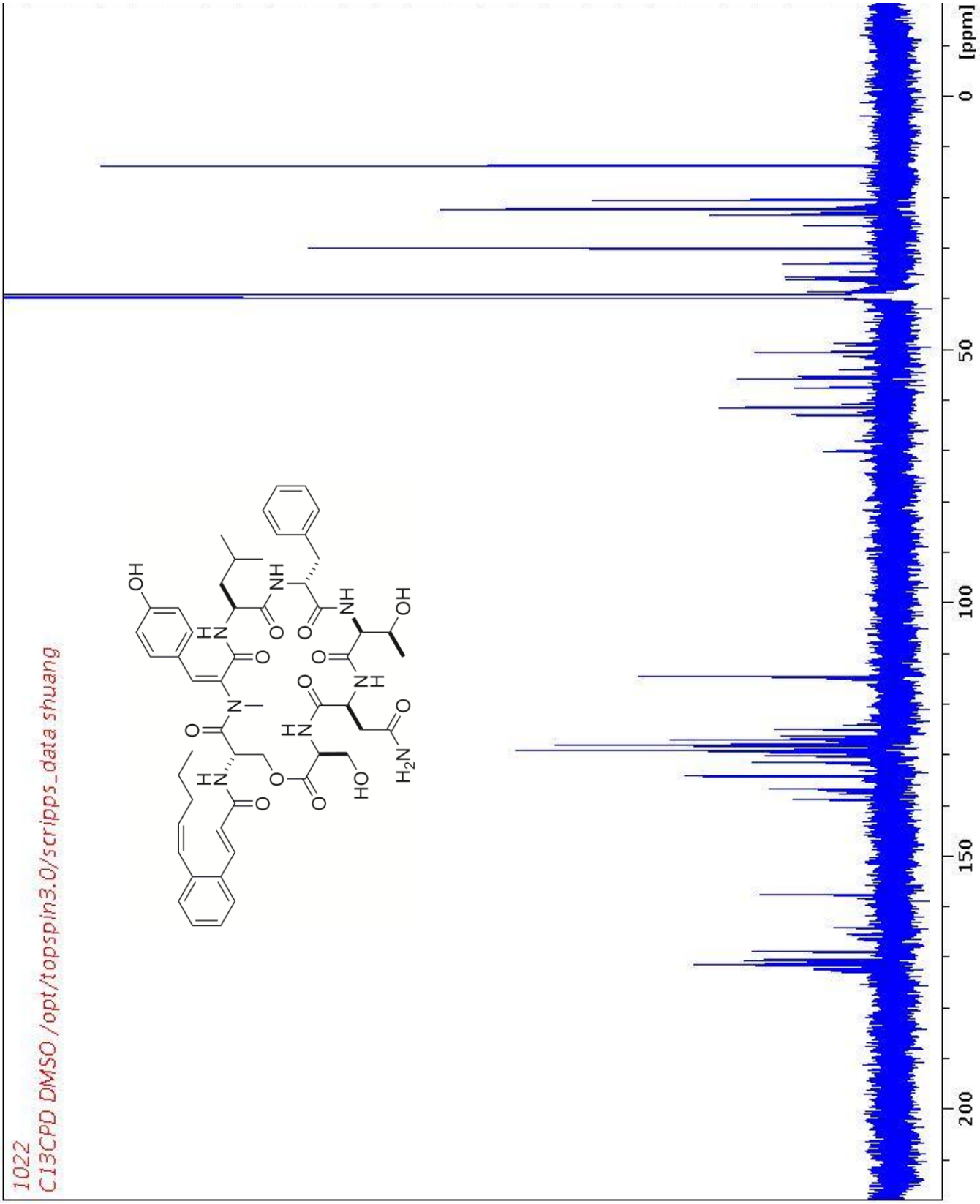

Figure S11. ^{1}H (700 MHz) NMR spectrum of triacetyl-WS9326C (**2a**) in $CDCl_3$

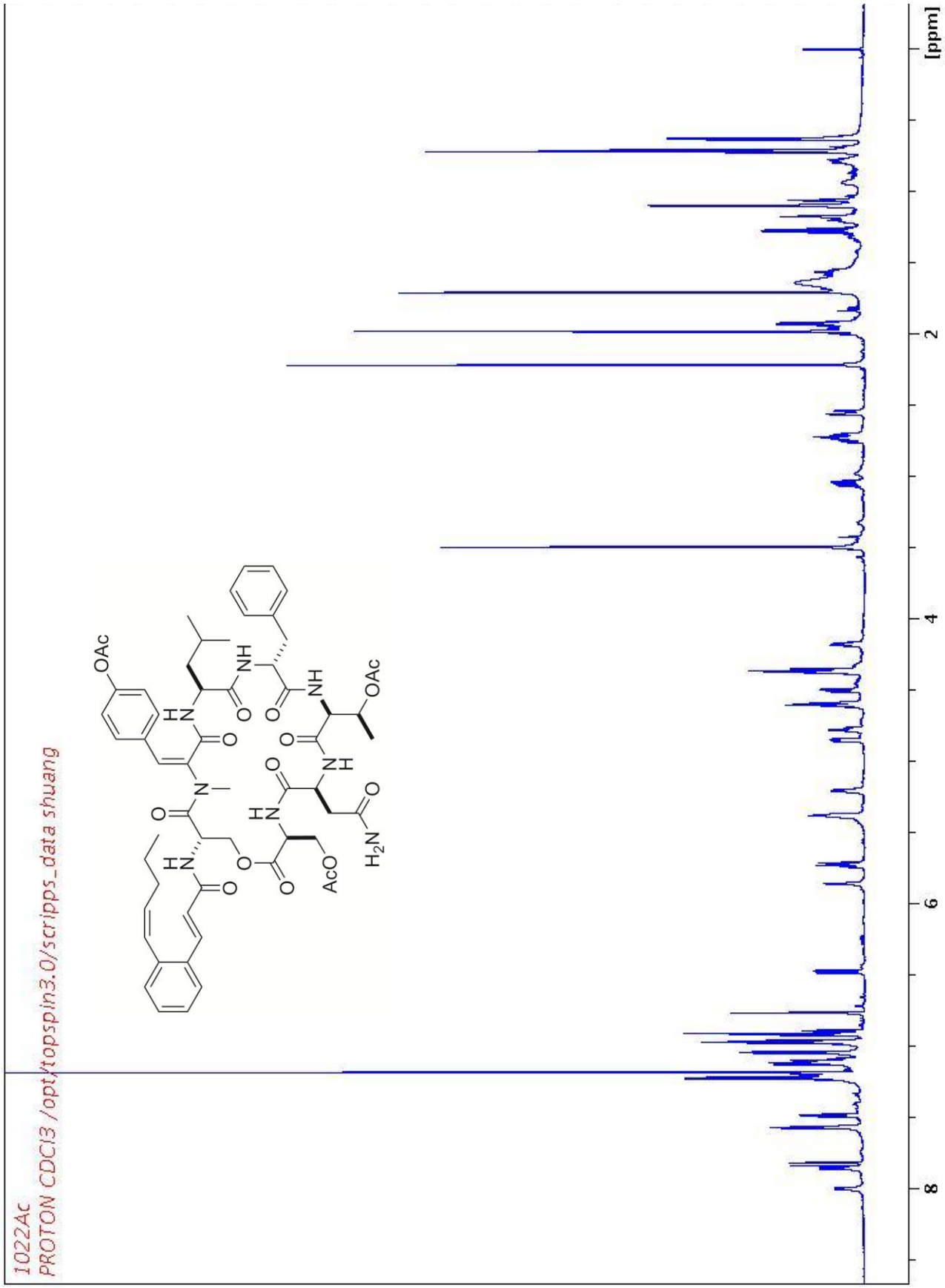

Figure S12. ^{13}C (175 MHz) NMR spectrum of triacetyl-WS9326C (**2a**) in $CDCl_3$

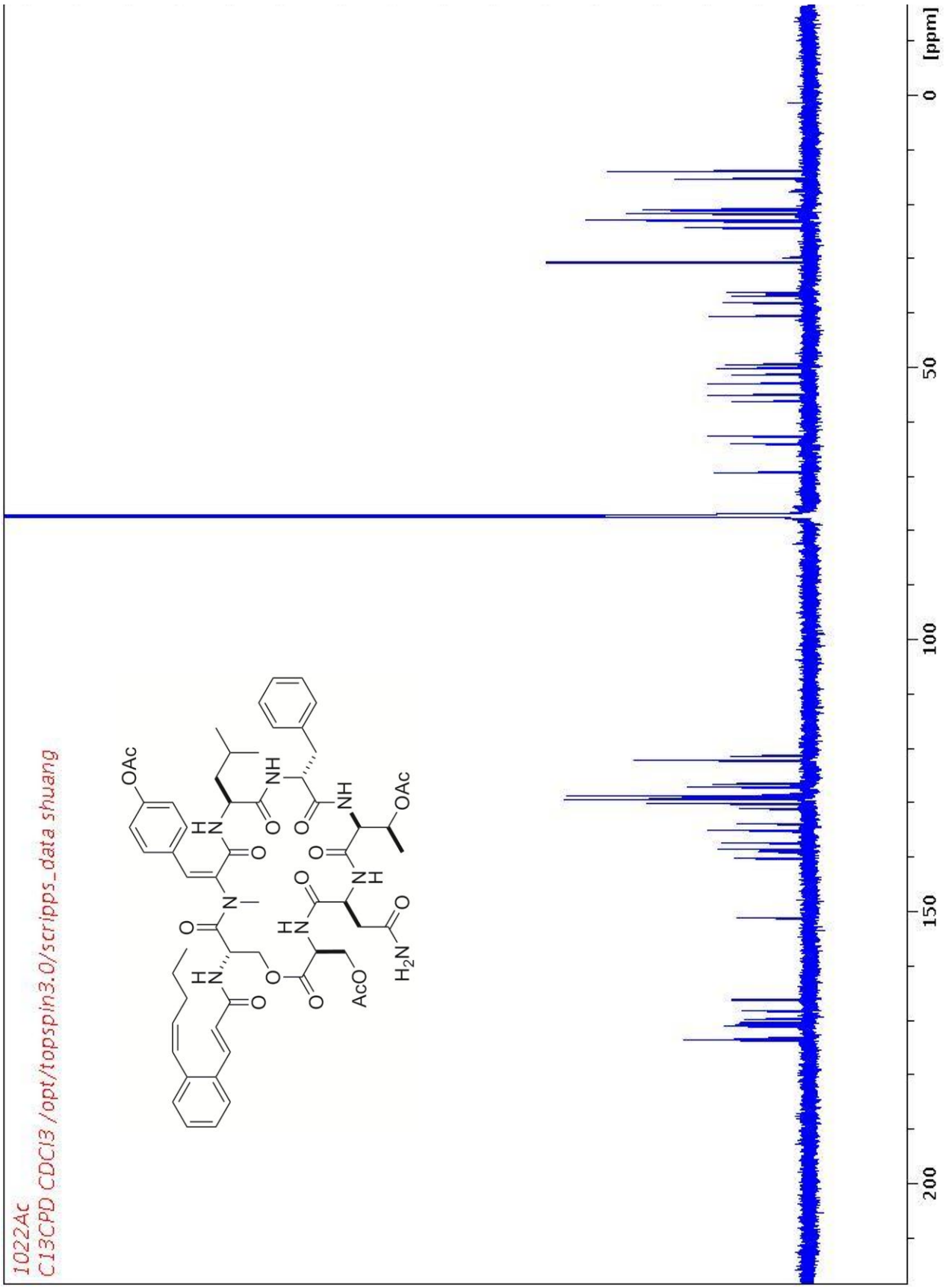

Figure S13. HSQC spectrum of triacetyl-WS9326C (**2a**) in $CDCl_3$

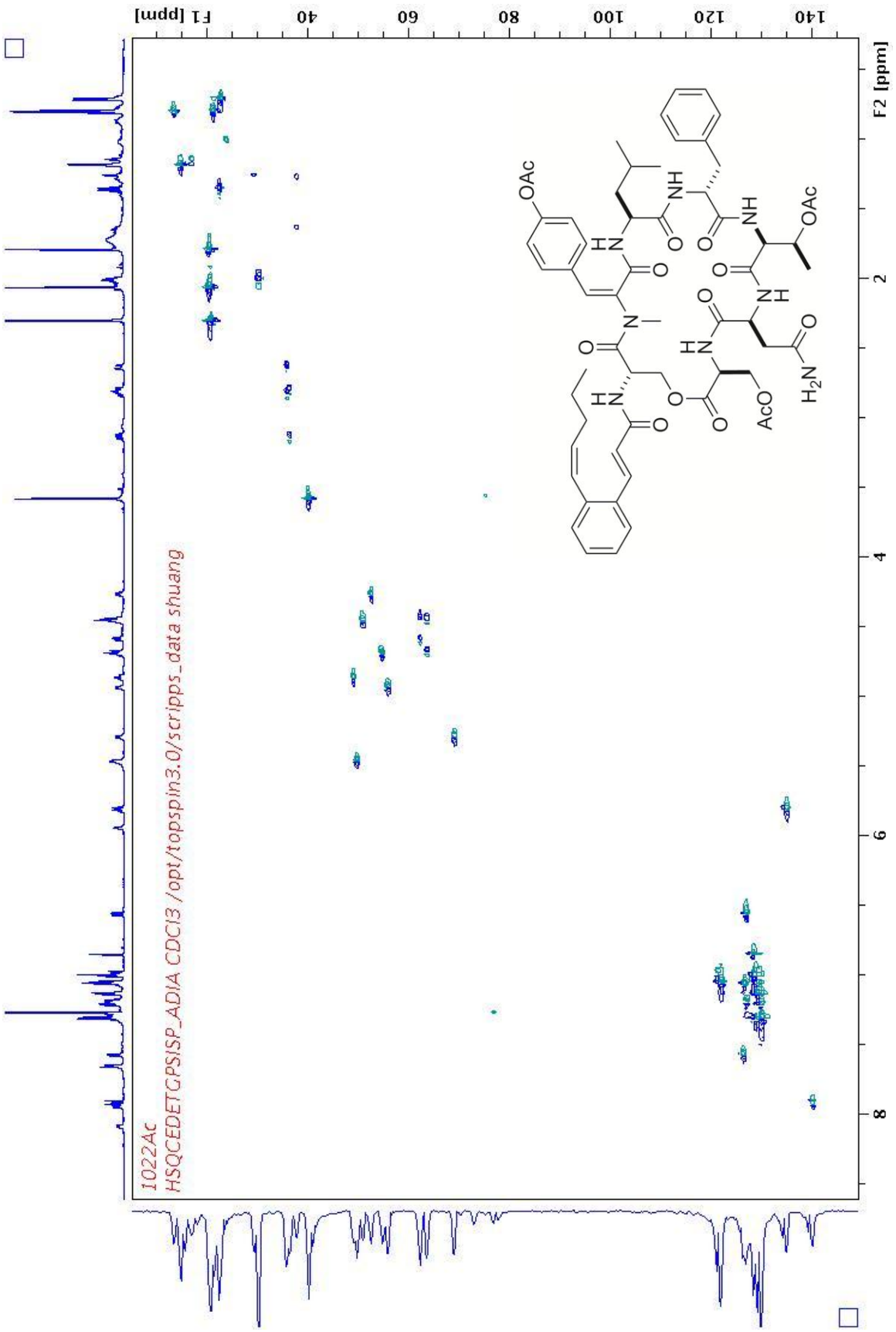

Figure S14. HMBC spectrum of triacetyl-WS9326C (**2a**) in $CDCl_3$

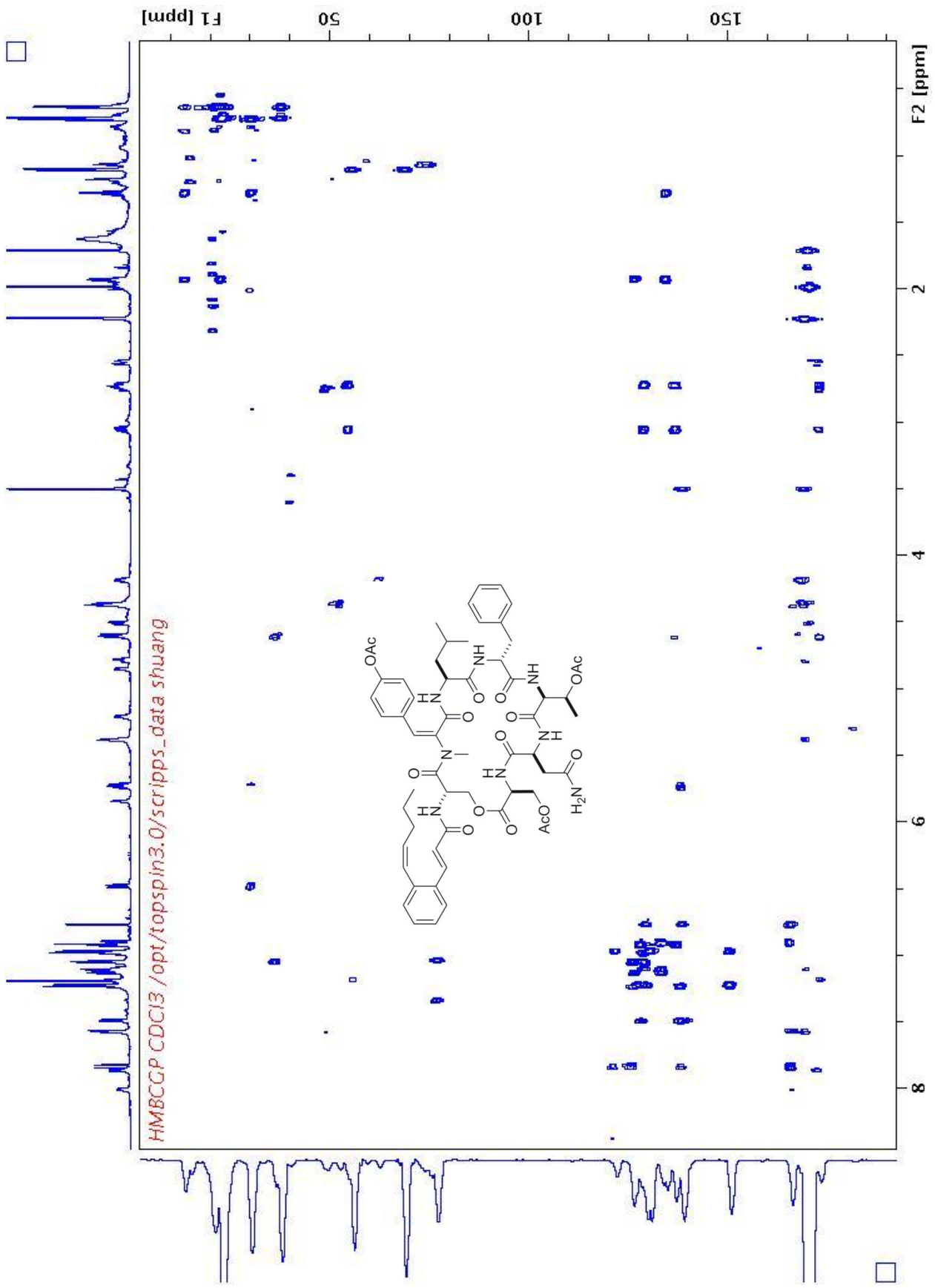

Figure S15. ^{1}H-^{1}H COSY spectrum of triacetyl-WS9326C (**2a**) in $CDCl_3$

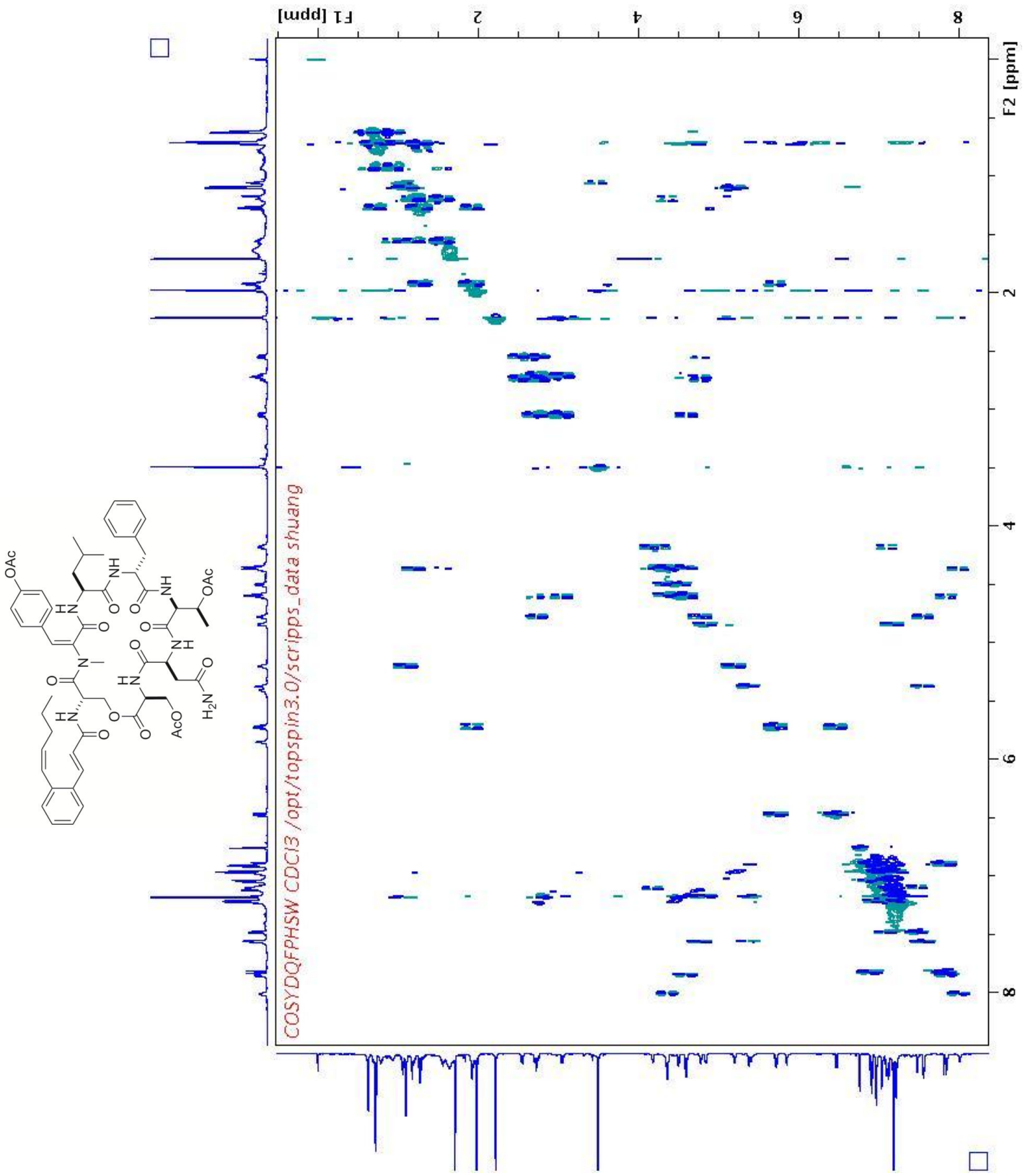

Figure S16. NOESY spectrum of triacetyl-WS9326C (**2a**) in $CDCl_3$

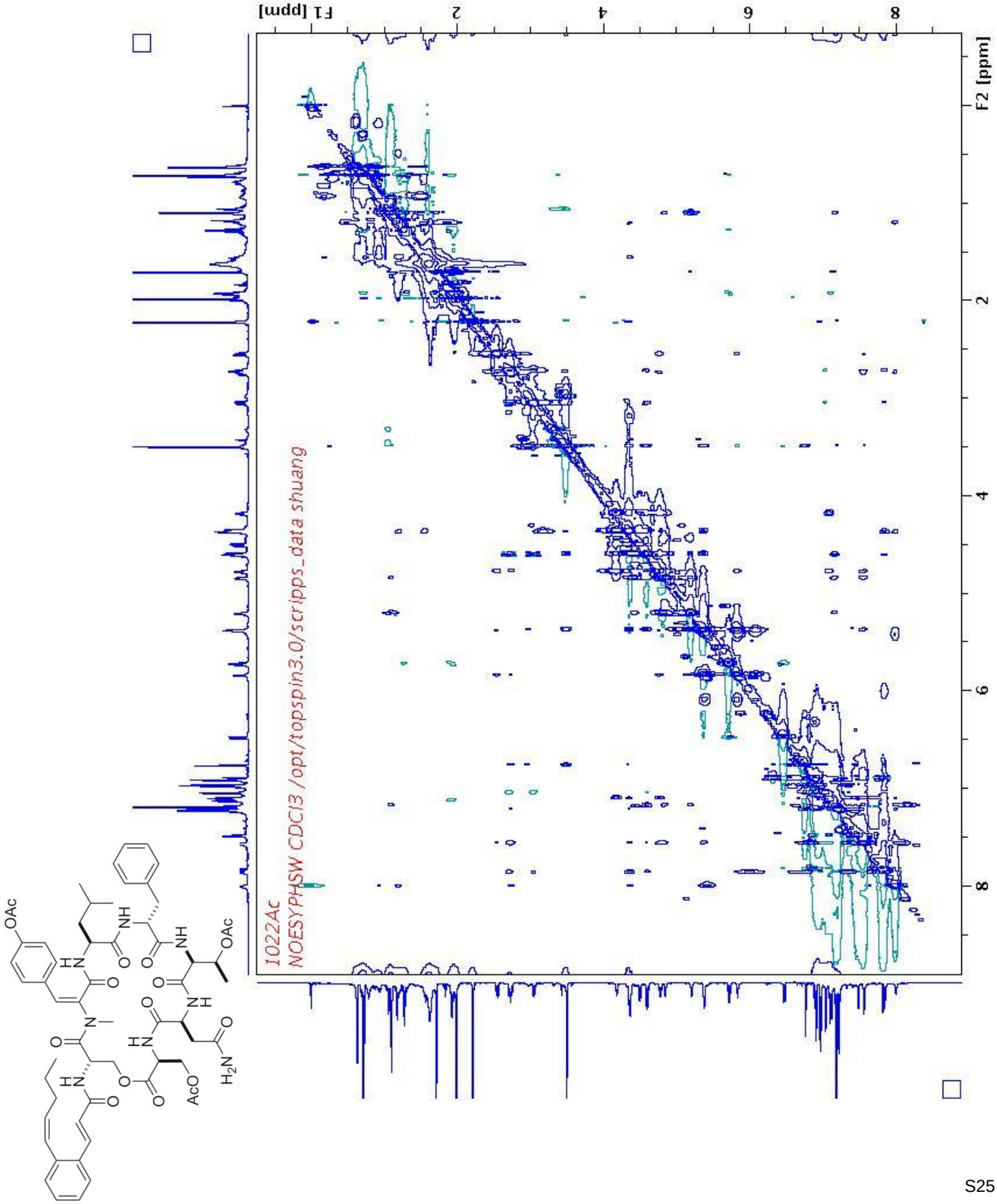

Figure S17. ^{1}H (175 MHz) NMR spectrum of WS9326D (**3**) in d_6-DMSO

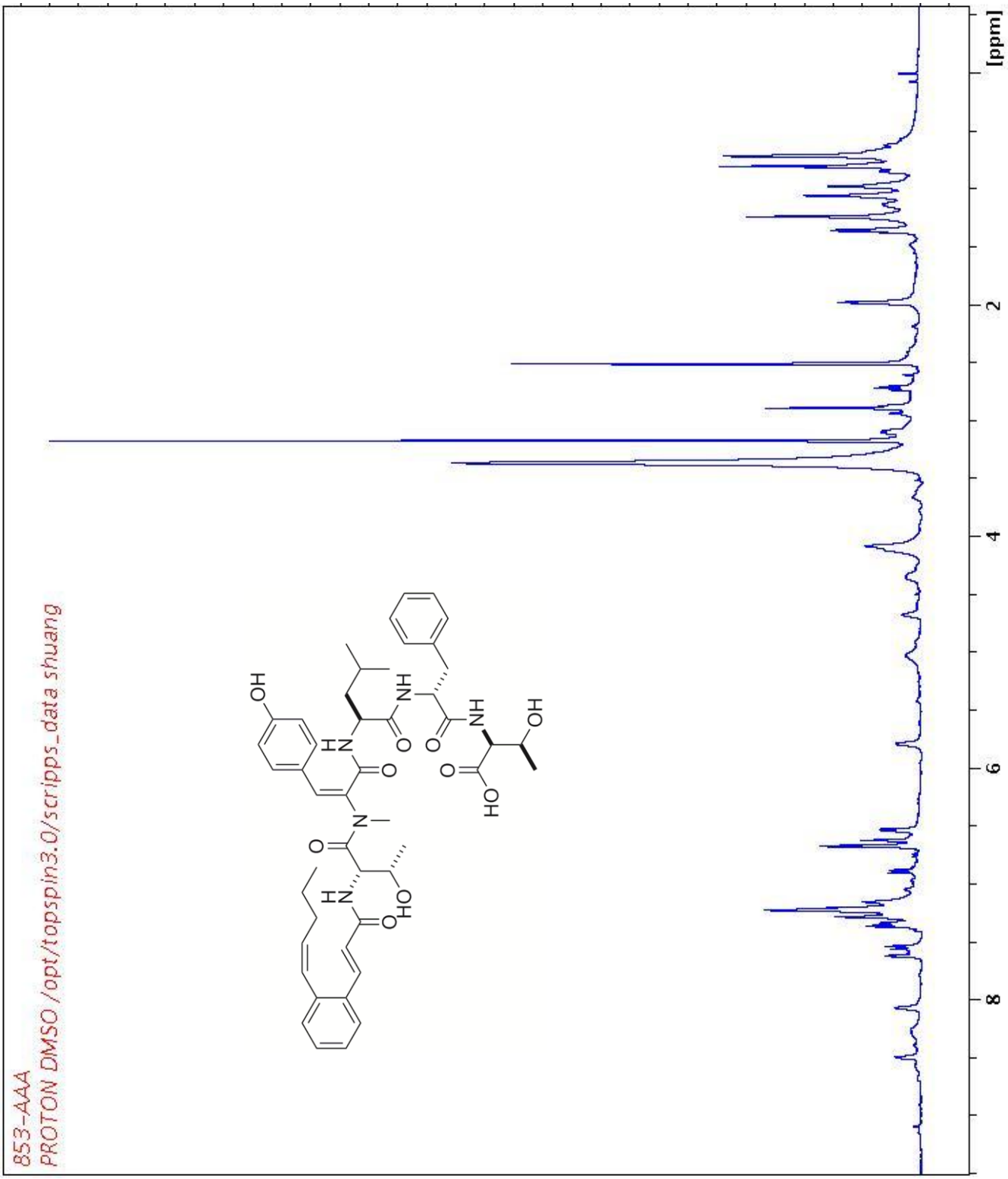

Figure S18. ^{13}C (175 MHz) NMR spectrum of WS9326D (**3**) in d_6-DMSO

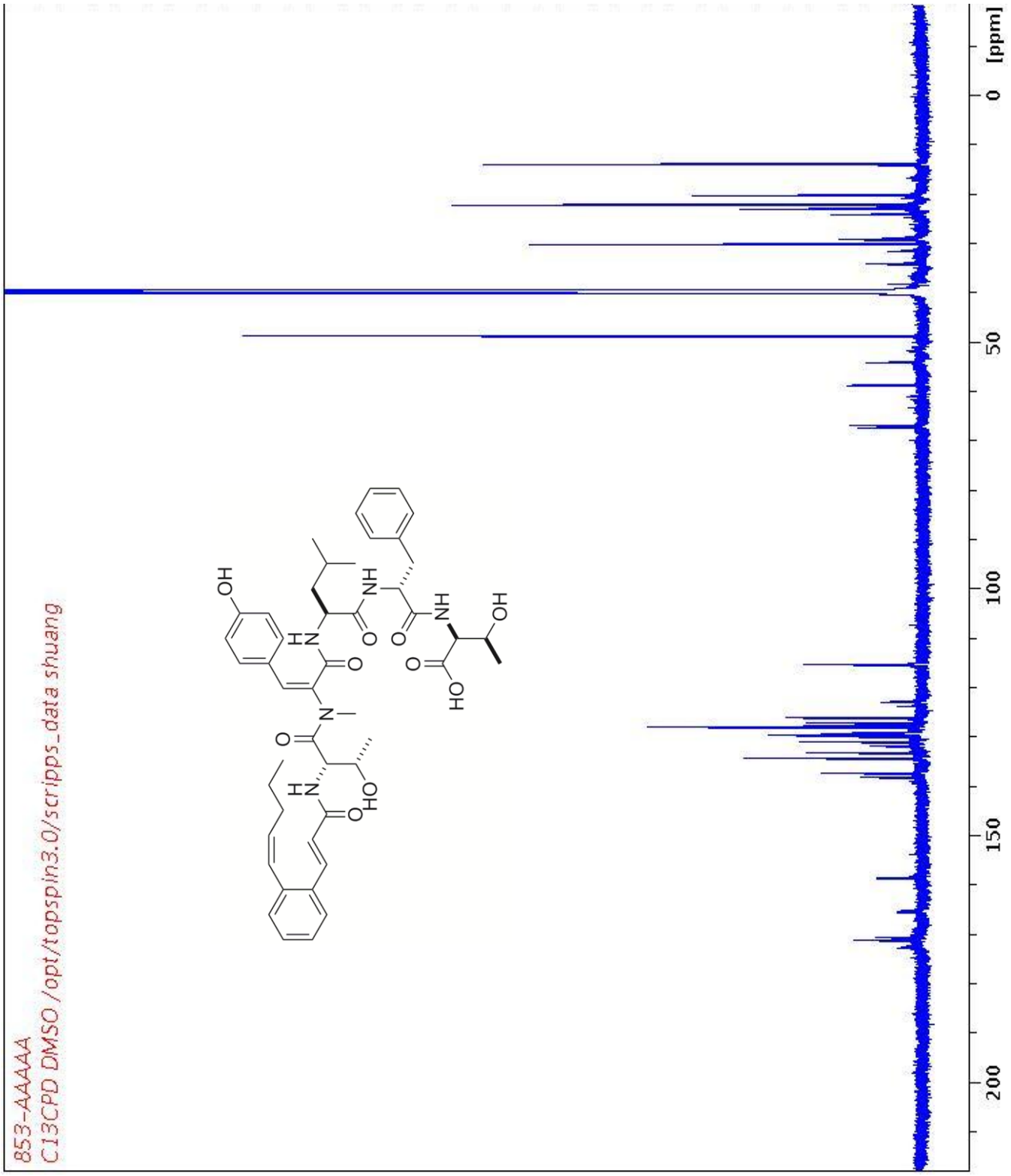

Figure S19. HSQC spectrum of WS9326D (**3**) in d_6-DMSO

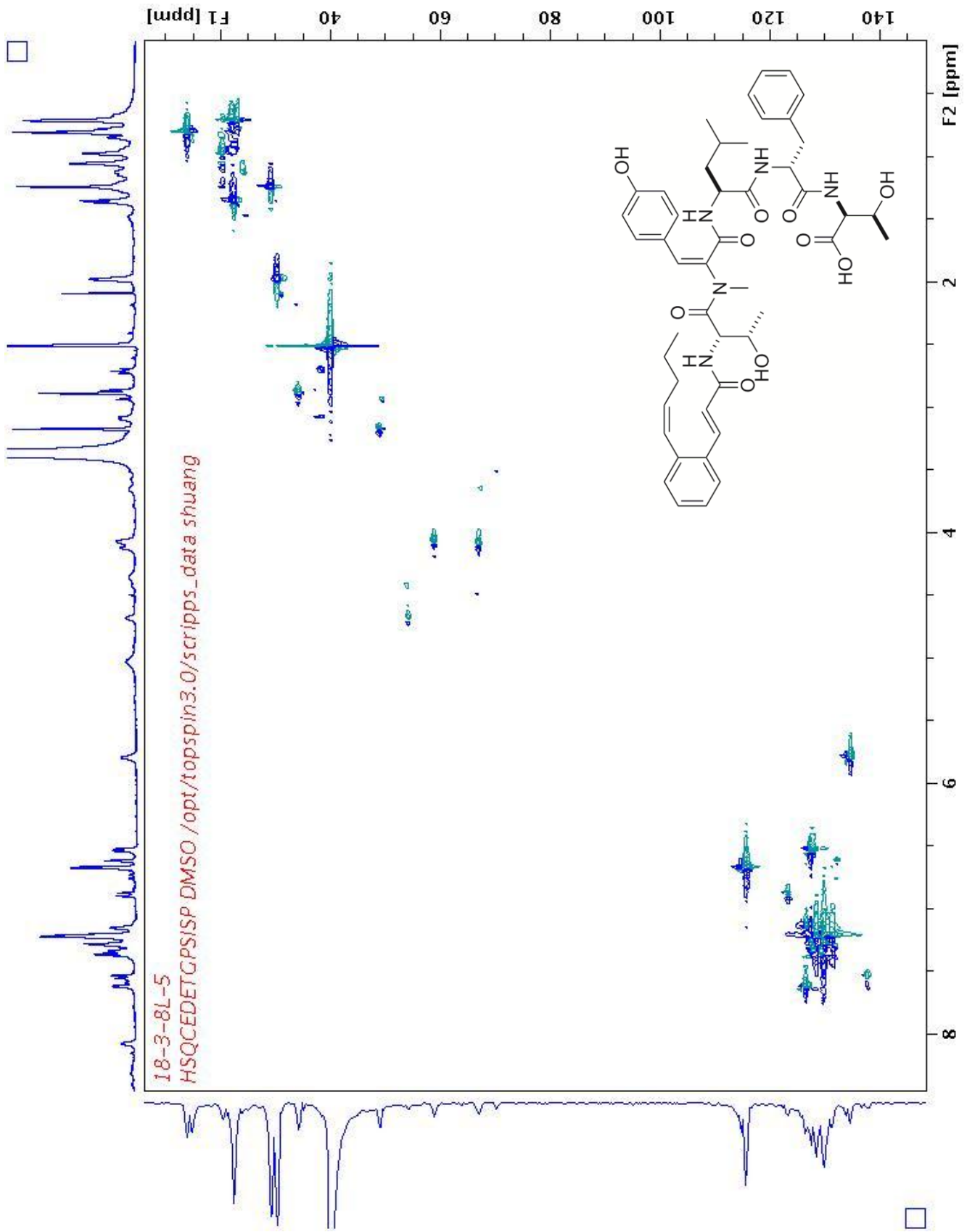

Figure S20. HMBC spectrum of WS9326D (**3**) in d_6-DMSO

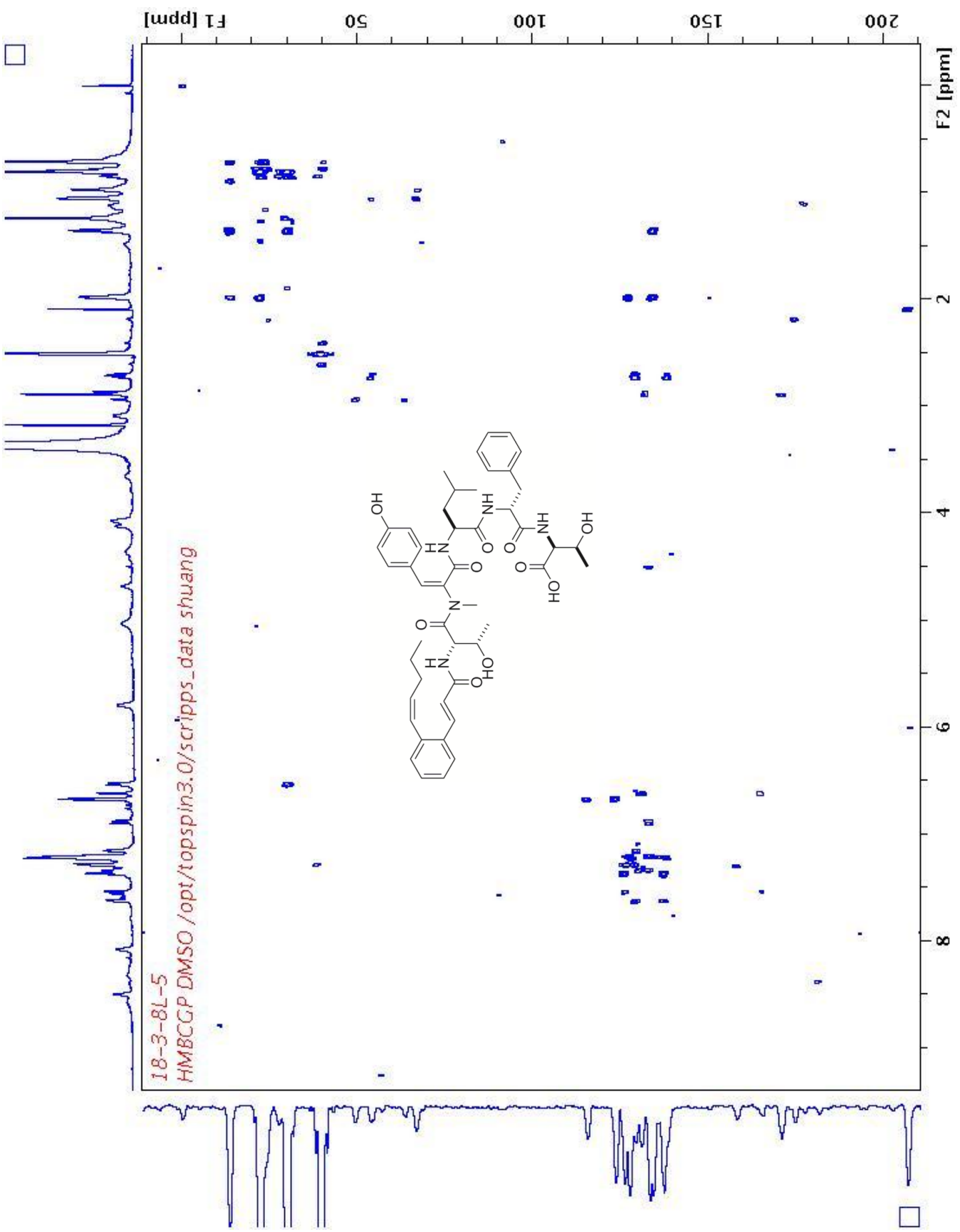

Figure S21. ^{1}H-^{1}H COSY spectrum of WS9326D (**3**) in d_6-DMSO

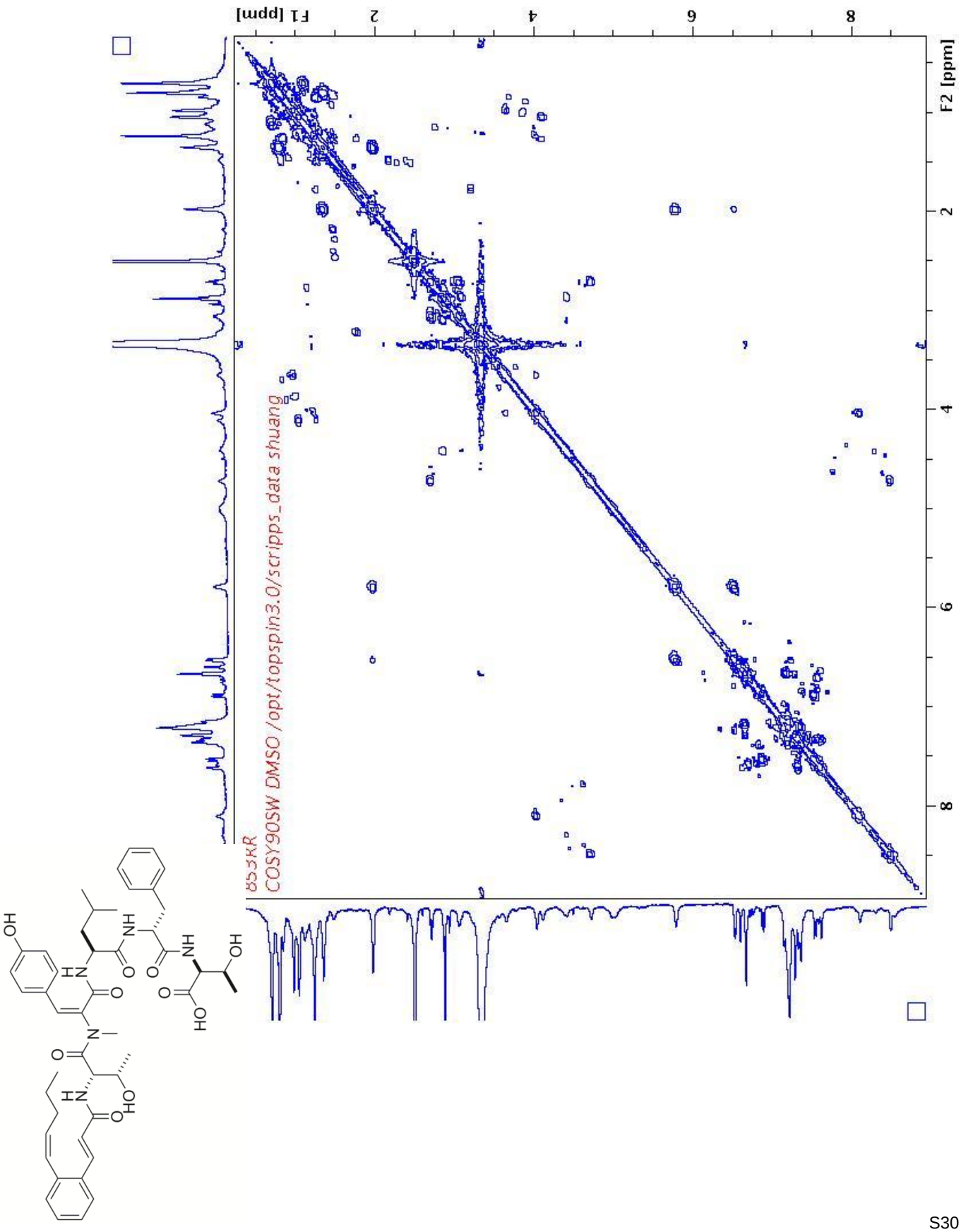

Figure S22. NOESY spectrum of WS9326D (**3**) in d_6-DMSO

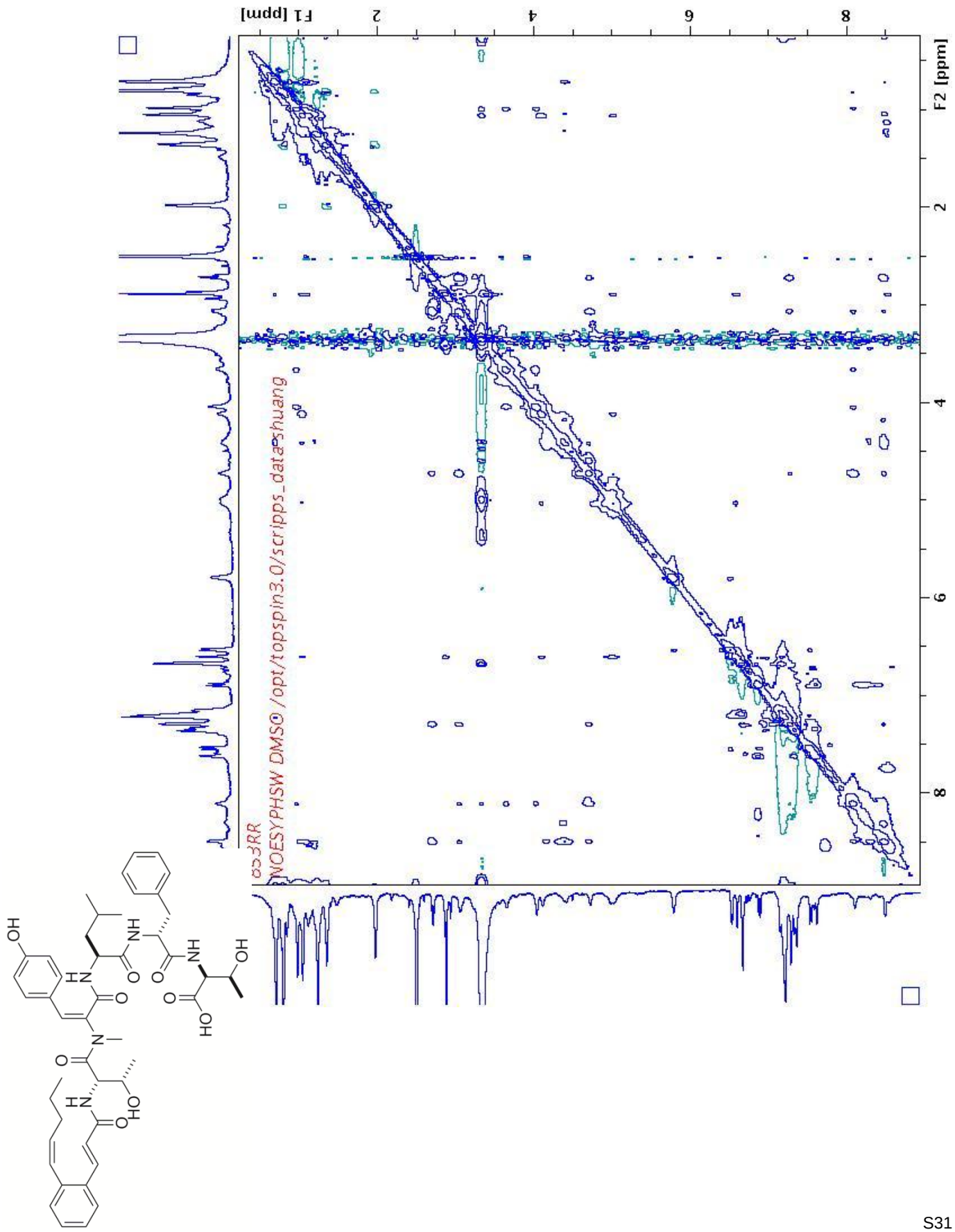

Figure S23. ^{1}H (700 MHz) NMR spectrum of WS9326E (**4**) in d_6-DMSO

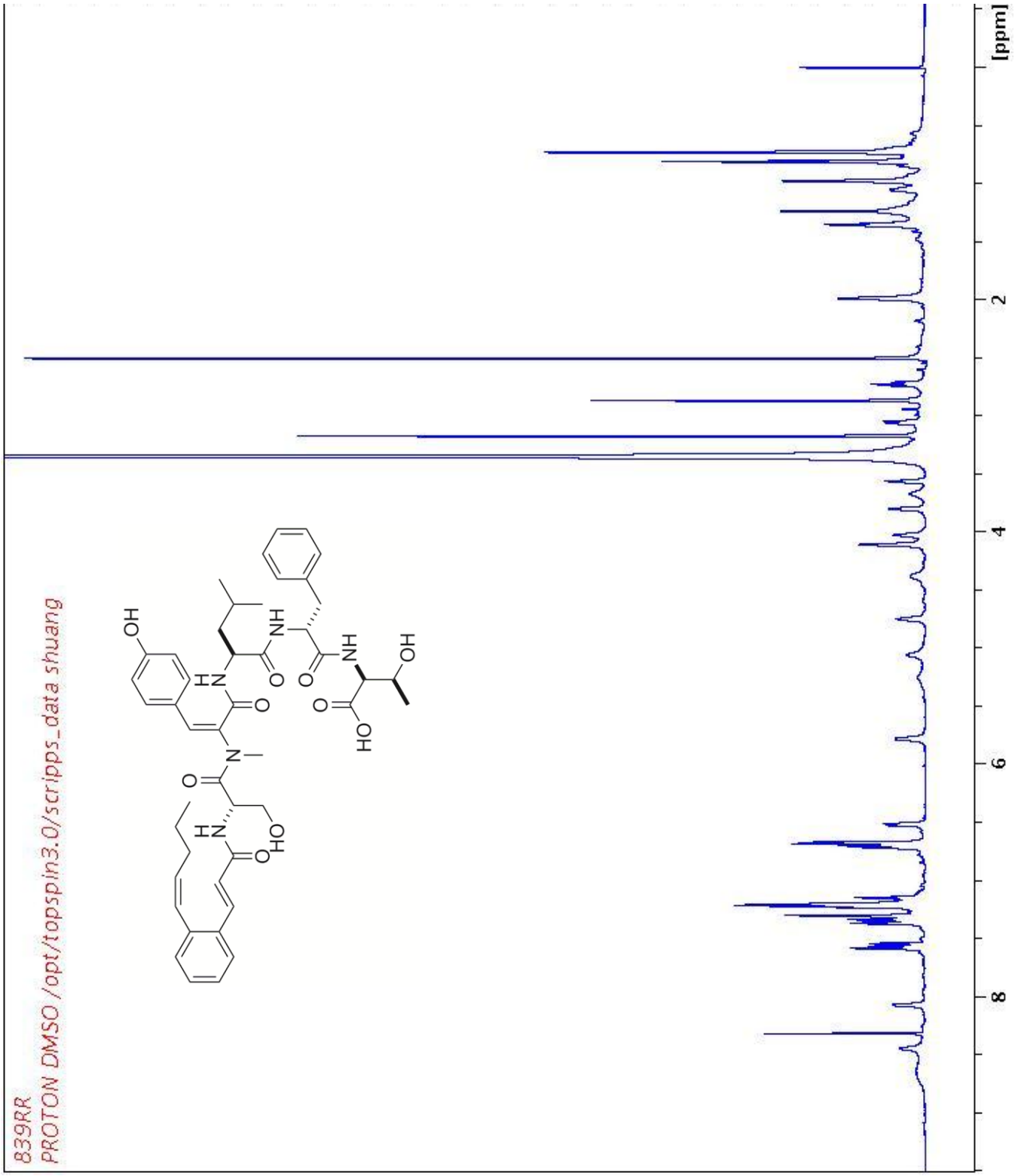

Figure S24. ^{13}C (175 MHz) NMR spectrum of WS9326E (**4**) in d_6-DMSO

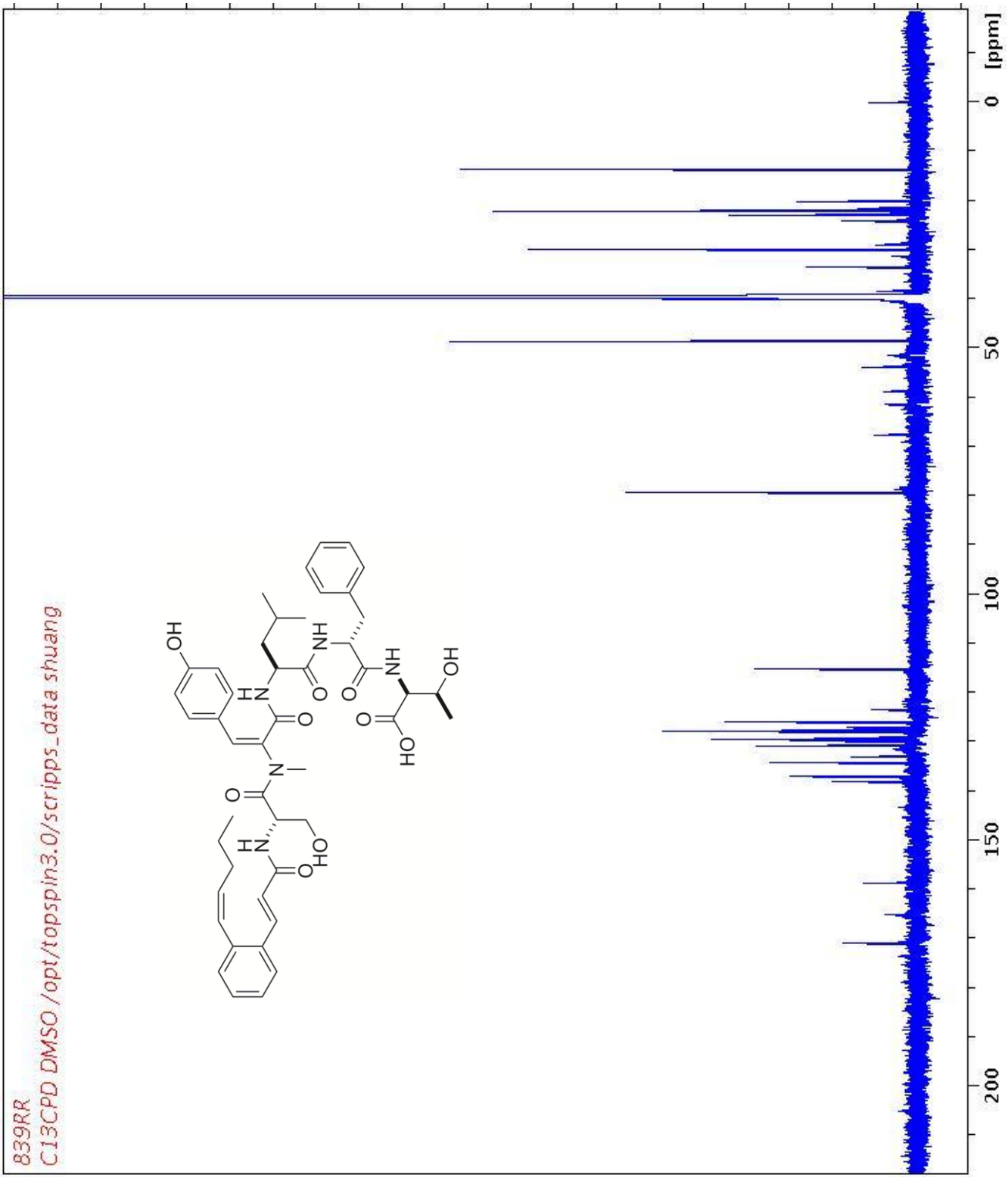

Figure S25. HSQC spectrum of WS9326E (**4**) in d_6-DMSO

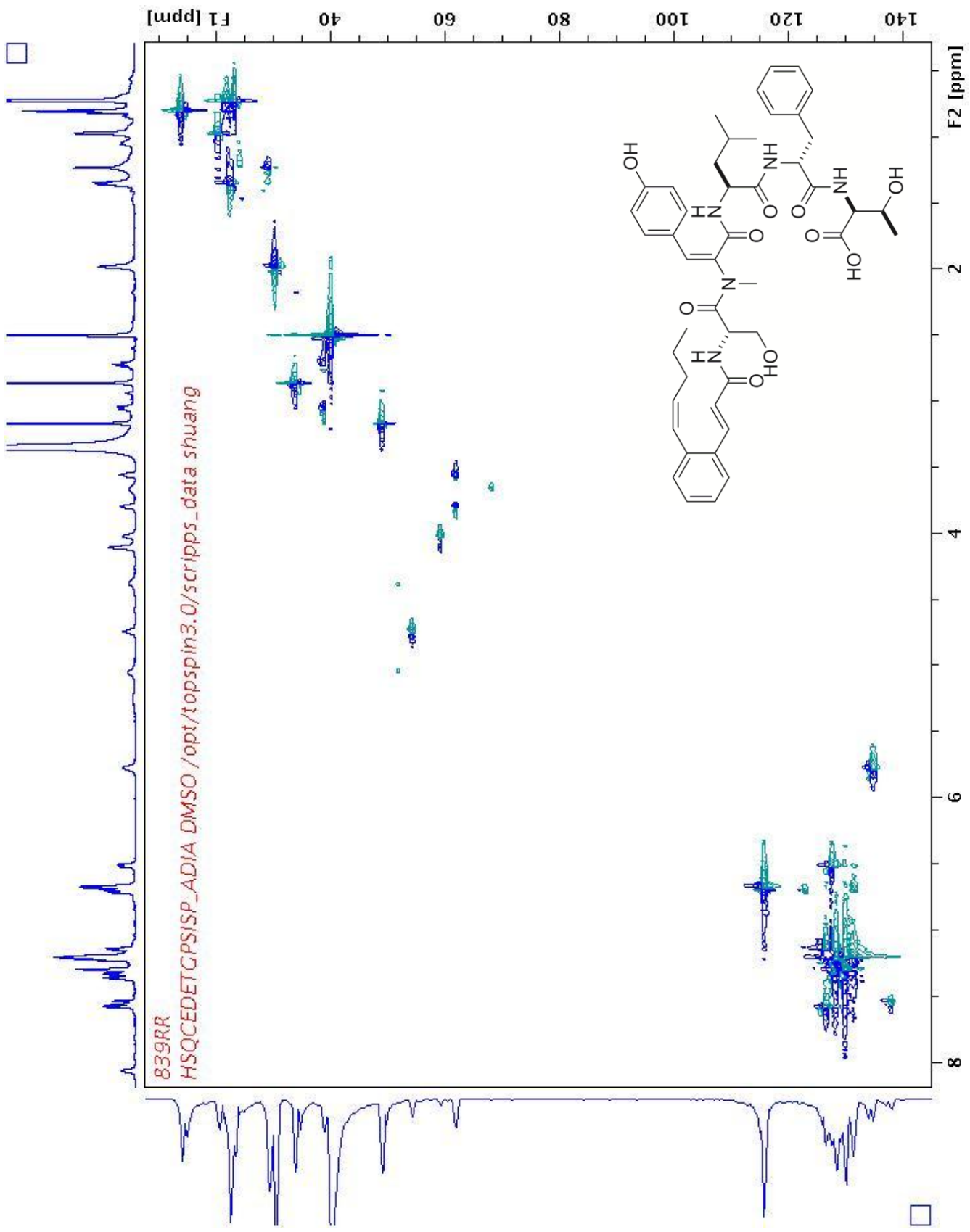

Figure S26. HMBC spectrum of WS9326E (**4**) in d_6-DMSO

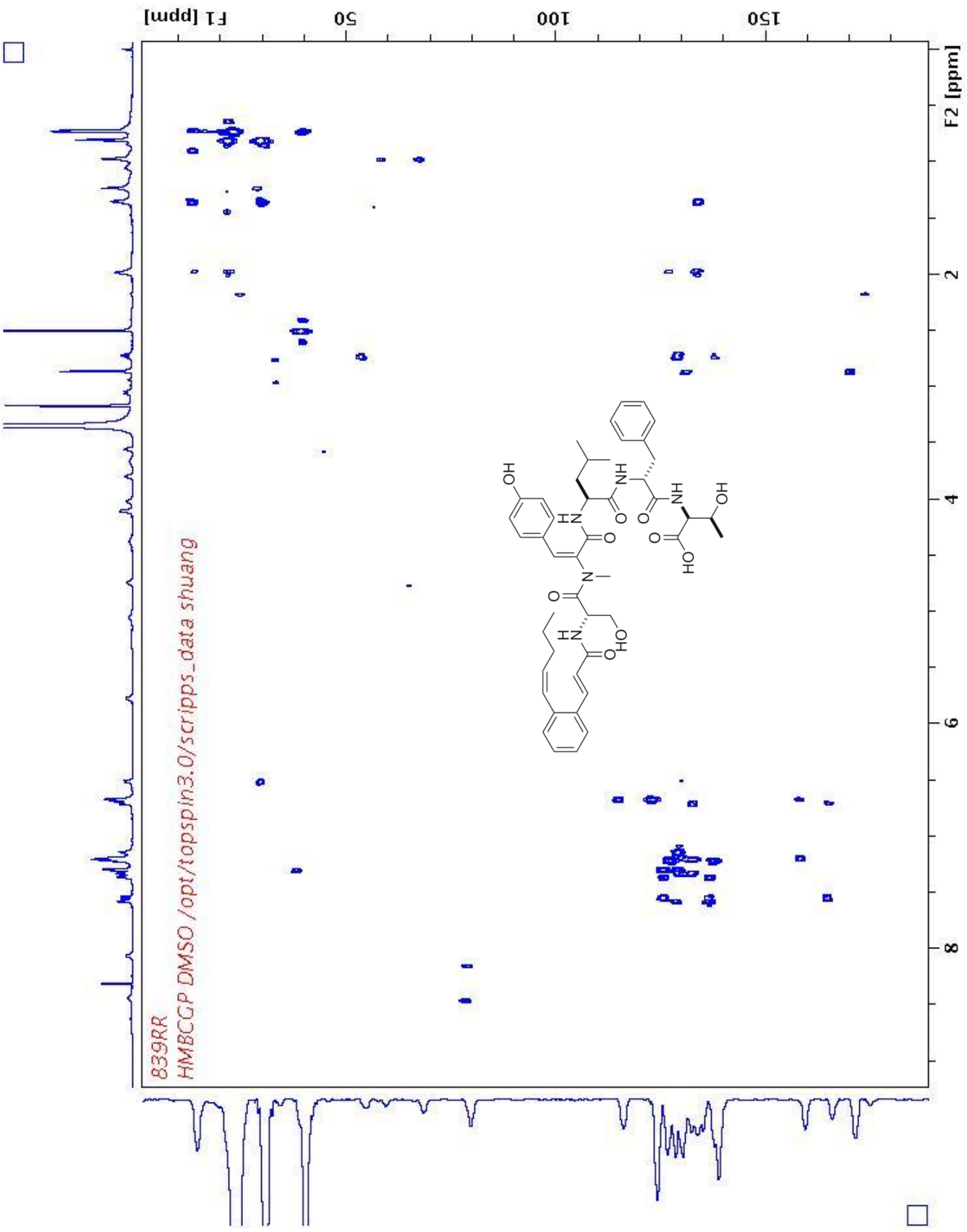

Figure S27. ^{1}H-^{1}H COSY spectrum of WS9326E (**4**) in d_6-DMSO

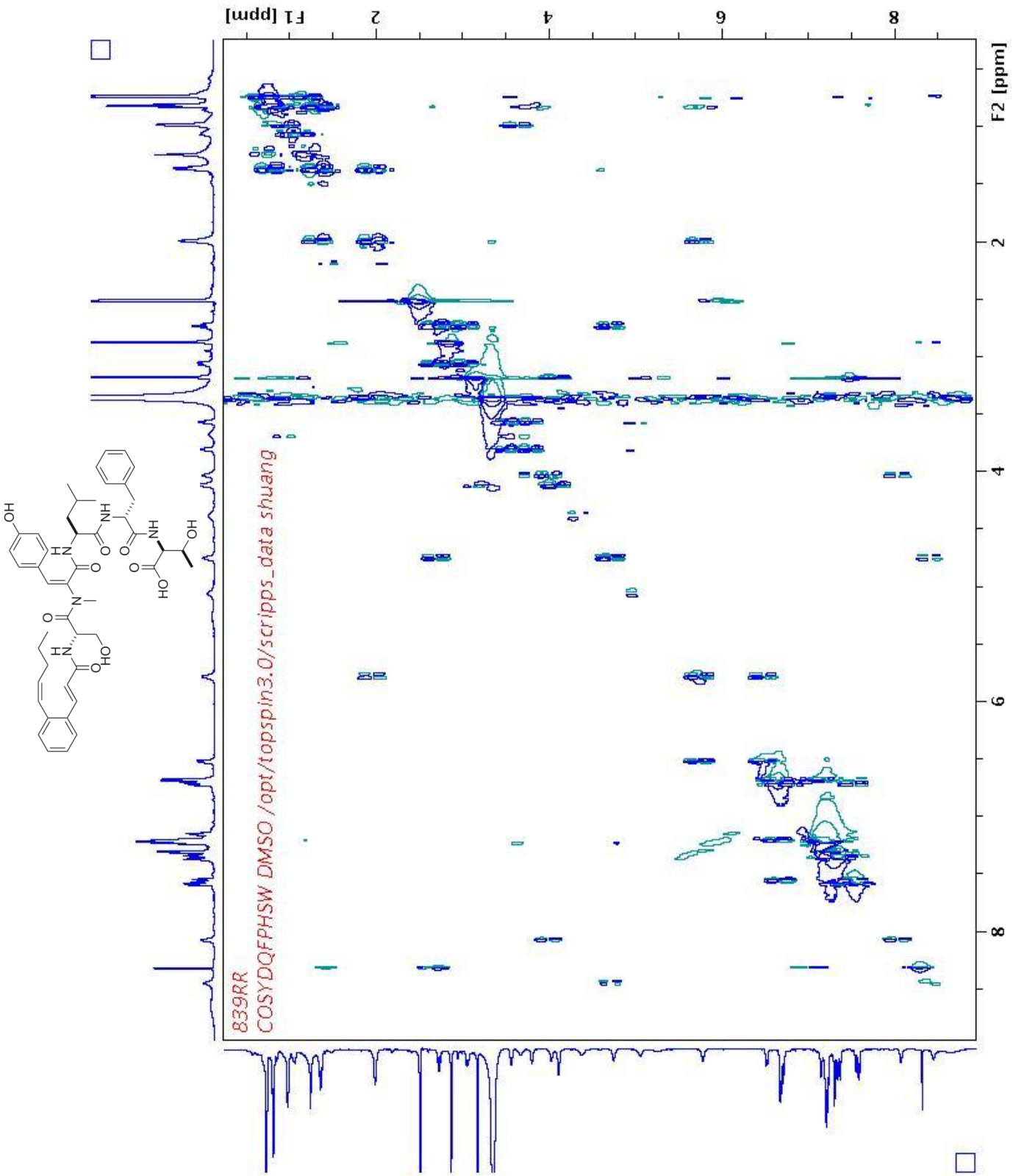

Figure S28. NOESY spectrum of WS9326E (**4**) in d_6-DMSO